Network Identification Capability Evaluation (NICE) of Regional Networks
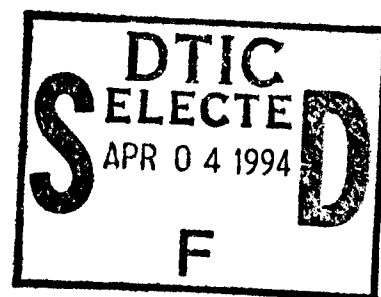
T. G. Barker, K. L. McLaughlin and J. L. Stevens

Maxwell S-CUBED Division
P.O. Box 1620
La Jolla, CA 92038-1620

DTIC
SELECTED
APR 0 4 1994
F

July 1994

Scientific Report No. 1

PHILLIPS LABORATORY
Directorate of Geophysics
AIR FORCE MATERIEL COMMAND
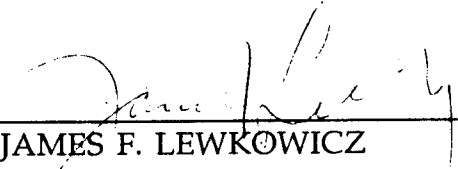**HANSCOM AIR FORCE BASE, MA 01731-3010**

19950403 022

DTIC QUALITY INSPECTED 1

The views and conclusions contained in this document are those of the authors and should not be interpreted as representing the official policies, either express or implied, of the Air Force or the U.S. Government.

This technical report has been reviewed and is approved for publication.

JAMES F. LEWKOWICZ
Contract Manager
Earth Sciences Division

JAMES F. LEWKOWICZ, Director
Earth Sciences Division

REPORT DOCUMENTATION PAGE

1. AGENCY USE ONLY *(Leave blank)*	2. REPORT DATE July 1994	3. REPORT TYPE AND DATES COVERED Scientific Report No. 1

4. TITLE AND SUBTITLE

Network Identification Capability Evaluation (NICE) of Regional Networks

5. FUNDING NUMBERS

Contract No: F19628-93-C-0177
PE 62301E

PR NM93   TA GM   WU AN

6. AUTHOR(S)

T. G. Barker, K. L. McLaughlin, and J. L. Stevens

7. PERFORMING ORGANIZATION NAME(S) AND ADDRESS(ES)

S-CUBED, A Division of Maxwell Laboratories, Inc.
P.O. Box 1620
La Jolla, CA 92038-1620

8. PERFORMING ORGANIZATION REPORT NUMBER

SSS-TR-94-14701

9. SPONSORING/MONITORING AGENCY NAME(S) AND ADDRESS(ES)

Phillips Laboratory
29 Randolph Road
Hanscom AFB, MA 01731-3010
Contract Manager: James Lewkowicz/GPEH

10. SPONSORING/MONITORING AGENCY REPORT NUMBER

PL-TR-94-2201

11. SUPPLEMENTARY NOTES

12a. DISTRIBUTION/AVAILABILITY STATEMENT

Approved for public release; distribution unilimited.

12b. DISTRIBUTION CODE

13. ABSTRACT *(Maximum 200 words)*

The computer program NICE, for Network Identification Capability Evaluation, was written to assess the ability of a seismic network to discriminate earthquakes from explosions. In this report on the progress during the first phase of a two-year project, we describe enhancements to the program which allow assessment of regional networks and discriminants. The enhanced program, called XCNICE simulates the detection, location and identification of a suite of events using a Monte Carlo approach. This approach allows one to isolate the effects of source type, propagation path, and choice of discriminants on the discrimination process. In addition, discriminant performance and network thresholds of detection, location and identification are assessed. The program has the capability to compute signals from earthquakes, quarry blasts and both overburied and normally buried explosions. The models of regional phases include the effects of nonlinear processes (continued)

14. SUBJECT TERMS

Seismic   Discrmination
Quarry Blast   Nuclear Explosion

15. NUMBER OF PAGES
50

16. PRICE CODE

17. SECURITY CLASSIFICATION OF REPORT	18. SECURITY CLASSIFICATION OF THIS PAGE	19. SECURITY CLASSIFICATION OF ABSTRACT	20. LIMITATION OF ABSTRACT
Unclassified	Unclassified	Unclassified	SAR

CLASSIFIED BY:

DECLASSIFY ON:

13. Abstract (Continued)

in particular, spall. We use kinematic models of spall to incorporate the effects of mass movemens associated with nuclear explosions and quarry blast charges. These spall movements change the source spectra, generally causing the measured slope above 1 Hz to increase. We use models of source spectra and the relative excitation of the sources to account for the differences in regional phase excitation for the various source types. We apply discriminants based on the spectral slopes from 1 Hz to 10 Hz of Lg, Pg and Lg/Pg to the events generated by XNICE. The models predict that spectral slopes for Lg, Pg and Lg/Pg are least for earthquakes, are greater for normally buried explosions and are greatest for quarry blasts. Spectral slopes of Lg are closer to earthquakes for overburied bombs, and can be indistinguishable at low magnitudes. These results are all consistent with numerous observations. We also show that network detection levels strongly influence these results.

Table of Contents

List of Illustrations

1. Introduction

The computer program NICE, for Network Identification Capability Evaluation, was written to assess the ability of a seismic network to discriminate earthquakes from explosions. In this report on the progress during the first phase of a two-year project, we describe enhancements to the program which allow assessment of regional networks and discriminants in addition to the original capabilities to assess teleseismic networks. The enhanced program, called XNICE (with an X windows interface) simulates the detection, location and identification of a suite of events using a Monte Carlo approach. This approach allows one to isolate the effects of source type, propagation path, and choice of discriminants on the discrimination process. In addition, discriminant performance and network thresholds of detection, location and identification are assessed. XNICE generates the parameters of a sequence of events and computes the ground motions from the events at the stations of the network. The features of the ground motions used for discrimination are then measured, and discrimination scores are assigned to each event. From a suite of events, the performance of the network and the discriminants can be assessed. The program has the capability to compute signals from earthquakes, quarry blasts and both overburied and normally buried explosions.

The models of regional phases (*Pn, Pg, Lg, Sn* and *Rg*) include the effects of non-linear processes, in particular, spall. We use kinematic models of spall to incorporate the effects of mass movements associated with nuclear explosions and quarry blast charges. These spall movements change the source spectra, generally causing the measured slope above 1 Hz to increase. We use models of source spectra and the relative excitation of the sources to account for the differences in regional phase excitation for the various source types. We apply discriminants based on the spectral slopes from 1 Hz to 10 Hz of *Lg*, *Pg* and *Lg/Pg* to the events generated by XNICE. The models predict that spectral slopes for *Lg*, *Pg* and *Lg/Pg* are least for earthquakes, are greater for normally buried explosions and are greatest for quarry blasts. Spectral slopes of *Lg* are closer to earthquakes for overburied bombs, and can be indistinguishable at low magnitudes. Spectral slopes are higher for normally buried bombs than for earthquakes due to the slope of (1) the spall source spectrum and (2) of the excitation spectrum of shallow explosions relative to mid-crustal earthquakes. Quarry blast spectral slopes are largest due to the effects of spall and of extended

source duration. These results are all consistent with numerous observations. Furthermore, we find that the population of spectral slopes of normally buried explosions separate from earthquakes more for an eastern U.S. earth structure than for the western structure. We also show that network detection levels strongly influence these results.

In addition, the X windows interface which has been installed is much easier to use than the question-and-answer format of the original program. In the following, we describe the architecture of the program, the means for doing regional analyses, and applications using western and eastern U.S. earth structures.

2. XNICE

2.1 Introduction

XNICE is comprised of four modules. The user communicates with the modules through the X interface, which also coordinates the modules. A flow chart of the system is shown in Figure 1. The modular design allows one to examine independently the effects of the seismic source, the wave propagation, the seismic network operation (location and detection) and discrimination rules on identification of events. The parameters of each module can be verified by direct comparison with observations. XNICE plots allow the user to examine a realization of the seismic events and details of the discrimination results. In addition, a link to the S-CUBED data visualization package *GeoSys* provides map drawings with contours and physical feature overlays.

2.1.1. EVENTS Module

The EVENTS module computes the source properties of a sequence of events which are realizations of probability distributions derived from observations of the source region. The distributions of earthquakes describe the epicenter, depth, moment, focal plane orientation and recurrence interval of the events. The program now computes source parameters for both overburied and normally buried explosions and quarry blasts. The parameters are chosen to be consistent with standard testing and quarrying practices, which are explained in Section 2.3. Nuclear explosions are specified by their yield, and in the case of overburied explosions, also by their depth of burial (a standard value of scaled depth of burial is assumed for normally buried explosions). Quarry blasts are specified

2

XNICE

X windows users's interface

events → synwave → analyst → examine → GeoSys

events

Source parameters

synwave

Waveforms, arrivals

analyst

Network bulletin

examine

Interactive graphics

GeoSys

Maps

Earthquakes:
Recurrence rates,
epicentral, depth
and focal mechanism
distributions.

Artificial Seismicity:
Location. depth. yield
distributions

Local propagation
Regional Propagation
Teleseismic propagation
Instrument responses
Noise levels
Station locations

Station locations
Detection rules
Location rules
Focal mechanism rules

Figure 1.   Flow chart of the XNICE system. The four major modules are controlled by the X windows interface. Graphic output can be supplied to GeoSys to make Graphics Information System (GIS) displays.

by their total yield. The results of the EVENTS module are written to a catalogue of events. Seismicity (natural and artificial) levels, depth and epicenter distributions are specified by files, which the user chooses with the X interface. The results of the EVENTS run can be viewed with a plotting module, which plots cumulative and incremental seismicity, event locations, depths and source sizes. The program can be run in two modes of operation: (1) a sequence of events with the random distributions discussed above, or (2) a fixed events occurring at nodes of a uniform grid of latitude and longitude. The second mode is used to generate contour maps of network detection and identification performance. The events bulletin can also be examined in lists of the bulletin which appear on the screen on demand ("pop-ups").

2.1.2. SYNWAVE Module

The SYNWAVE module is a synthetic seismogram package. It reads the events catalogue generated by the EVENTS module and station locations and detection level parameters from a station file and computes synthetic teleseismic body wave (P, pP and S phases) and fundamental-mode surface wave seismograms for the network, and amplitudes of regional phases (Pn, Pg, Sn, Sg, Lg) at a set of prescribed frequencies. The calculation of regional amplitudes is discussed in Sections 2.2 through 2.4. Discrimination methods use measurements of peak amplitude, spectral amplitude, period and travel time, which the program models by incorporating the most important physical effects. The signals depend upon the source spectrum (which depends on the moment), instrument response, source depth, anelastic attenuation, and, for surface waves, dispersion. The amplitude depends upon source strength, radiation pattern, geometric spreading and anelastic attenuation. The signals are measured for amplitude, period and travel time after which random noise is added to the measurements. Signals which do not meet a specified signal-to-noise ratio are classified as non-detections. An arrival bulletin is then written to a file. The parameters of wave propagation can be regionalized and verified by comparison with observations. The user specifies the bulletin names and propagation files through the X interface. The arrival bulletins can be examined in pop-up lists.

2.1.3. ANALYST Module

The ANALYST module reads the arrival bulletin made by the SYNWAVE module and does calculations based upon network analysis. The

4

calculations include assignment of discrimination scores, network averaged m_b, M_s and regional magnitudes, such as $m_b(Lg)$. The ANALYST module computes the scores for these teleseismic discriminants: epicentral location, depth by pP, depth by travel times and ratio of m_b to M_s. We have now included regional discriminants based on spectral amplitudes and slopes used in discriminants such as the ratio of high to low frequency Lg. We show examples of the application of regional discriminants in Section 4. The program uses teleseismic rules similar to those of AFTAC for censoring bad data (rejection of signals based on signal-to-noise ratios and number of quadrants reporting) and for assigning discrimination scores, which indicate the degree of confidence that the event can be considered an earthquake. The results of the calculations by the ANALYST module are written to a discrimination bulletin file.

2.1.4. EXAMINE Module

The EXAMINE module makes lists and plots which allow the user to examine interactively the discrimination bulletin and the identification performance of the network. An X interface allows the user to view not only the overall performance, but also features of the process which contributed to the performance. For example, one may determine the identification rate as a function of m_b. In addition, discrimination bulletins can be compared with this module. Thus, the results of a Monte Carlo simulation can be compared with a bulletin derived directly from observations so that the program can be calibrated for a particular seismic area and network. An extensive menu of plots and lists are available to the user through the X interface.

2.2 Regional Propagation Modeling

Details of modeling teleseismic discrimination in NICE are given in Barker and Rodi (1986). Normally buried explosions, overburied explosions and quarry blasts have been added to the teleseismic code (see Barker, *et. al.*, 1993 for the body wave formulations). In this report, we describe the regional processing added to XNICE. The reader is referred to Barker and Rodi (1986) for details on modeling teleseismic phases by NICE. A number of authors have derived empirical or heuristic expressions of regional phase propagation (see, for example, Goncz, *et. al.*, 1986 or Nuttli, 1975). We use a form, modified from Campillo, *et. al.* (1985), which includes the effects of propagation and source excitation explicitly. The observed signal amplitude (peak narrow-bandpass or

spectrally averaged amplitude) at range Δ and frequency f has the form:

$$A(f,\Delta) = \Omega(f)\,\hat{G}(\Delta,f),$$
$$\hat{G}(f,\Delta) = E(f)\,P(\Delta,f),\qquad\qquad (1)$$

where $\Omega(f)$ is the source spectrum. The function $\hat{G}(f,\Delta)$ is an effective Green's function comprised of $E(f)$, the source excitation spectrum and a propagation term, specified by

$$log(P(\Delta,f)) = -n\,log(\Delta/\Delta_0) + log(e)\gamma(f)(\Delta - \Delta_0) + \varepsilon\,,$$

where Δ_0 is a reference distance, $\gamma(f)$ is the anelastic attenuation parameter, n is a factor for geometric spreading (typically $n = 5/6$), and ε incorporates random effects of local station response and noise. The source excitation spectrum $E(f)$ depends on source type (earthquake, explosion, etc.) and source depth. The source excitation spectra are calibrated from calculations of synthetic seismograms or from observations of signals from different sources along common paths. The basic assumption underlying this approach in XNICE is that differences in spectral slopes for different types of sources and waves (Lg, Pg) are caused by differences in source $\Omega(f)$ and excitation $E(f)$. In the following, we describe these source and excitation functions in detail.

2.3   Source Spectra

XNICE computes signals from four source types: earthquakes, quarry blasts, and both overburied and normally buried explosions. Earthquake source spectra have been thoroughly studied. For large events ($m_b > 5$), spectra are quite complicated at frequencies above 1 Hz. For smaller events, however, there is general agreement that a good model for the source spectrum is flat at low frequencies, and rolls off as f^{-2} at frequencies above a corner which is proportional to the cube root of the moment divided by the stress drop. For events in the range $2.5 < m_b < 4$, the effects of changing the corner frequency with magnitude or moment changes the ratio of low (near 1 Hz) to high frequency amplitudes (> 1 Hz). The formulation by Brune (1970) is implemented in XNICE:

6

$$\Omega_{eqk} = \frac{M_0}{1+(f/f_c)^2}$$

$$f_c = \left(\frac{\sigma}{M_0}\right)^{1/3}\beta^{-1}$$

where σ is the stress drop and M_0 is the static moment. Distributions of source parameters (recurrence intervals, epicenter, depth, fault plane orientation, and moment) are specified on files as described in Barker and Rodi (1986), while the interface allows the user to specify the number of events in the ensemble, or the number of years of natural seismicity. The mean stress drop is set to be 10^7 Pa (100 bars) and varies randomly over a uniform range of +/- 20%. The amplitude of the signals from an earthquake is simply

$$A_{eqk}(f,\Delta) = \Omega_{eqk}(f)E_{eqk}(M_0,f)P(\Delta,f) \quad ,$$

We discuss the calculation of E_{eqk} in the next subsection.

Nuclear explosion source spectra have also been studied extensively. XNICE uses the equations given by Mueller and Murphy (1971). Like earthquakes, the spectra are flat at low frequencies and decrease as f^{-2} at high frequencies. The parameters of the Mueller-Murphy source are explosive yield, material type and depth of burial. Normally buried explosions are observed to interact non-linearly with the free surface, producing spall and appreciable secondary regional signals (e.g., Taylor and Randall, 1989). McLaughlin, *et. al.* (1988) show that two-dimensional effects such as spall must be added to a simple point source to match Lg excitation. Day, *et. al.* (1983) proposed that the spall phase be modeled as a horizontal tension crack, and Barker and Day (1990) showed that the two-dimensional simulations of explosions fit the model in the frequency band of 1 to 10 Hz. Recently, Patton and Taylor (1993) found that the tension crack model could be used to fit Lg spectral ratios from NTS explosions. The tension crack model is parameterized by the depth and radius of the crack and the distribution of velocities at which material moves upward from the crack (or equivalently, the spall mass and momentum). The parameters found by Barker and Day (1990) were consistent with near-field observations of spall summarized by Patton (1989). There is considerable scatter in those parameters and we use averages found from regressions in Patton (1989). In XNICE, we model the spall time history as

$$\Omega_{spall}(t) = m_{spall}\left[v_0\delta(t) + (gt_d - v_0)\delta(t - t_d) - g(H(t) - H(t - t_d)) \right] , \qquad (3)$$

where v_0 is the detachment velocity (assumed constant over the tension crack surface), g is the acceleration due to gravity, t_d is the dwell time

$$t_d = 2v_0/g ,$$

and δ and H are the Dirac delta and Heaviside functions. For an overburied explosion, the user specifies the source material and depth of burial and a range of yields. For a normally buried explosion, a depth of burial of

$$z_b = 125\ W^{1/3}$$

where the W is the yield in kilotons, is assumed (in these and subsequent formulas, all units are SI, unless otherwise specified). Following Patton (1989), the detachment velocity is found from

$$v_0 = 5 x 10^3 z_b^{1.6}$$

and the spall mass is

$$m_{spall} = 10^{10}W .$$

Barker and Day (1990) show that the spall signal for normally buried explosions is strongly peaked near a frequency equal to $1/t_d$, which is typically near 1 Hz. For the overburied explosion, the amplitudes are computed from

$$A_{obex}(f,\Delta) = \hat{G}_{exp}(h,f)\Omega_{exp}(W,f)\,P(\Delta,f) , \qquad (4)$$

where $\hat{G}_{exp}$ is the amplitude of the Green's function for an isotropic source, and Ω_{exp} is the Mueller-Murphy source spectrum. The amplitude for a normally buried explosion is

$$A_{nbex}(f,\Delta) = \left[\hat{G}_{exp}(f)\Omega_{exp}(W,f) + \hat{G}_{vf}(f)\Omega_{spall}(W,f) \right]T(\Delta,f)$$
$$\hat{G}_{vf}(f) = E_{vf}(f)P(\Delta,f) . \qquad (5)$$

Here, $\hat{G}_{vf}(f)$ is the Green's function for a vertical force on the free surface. Day and McLaughlin (1991) show that for wavelengths long compared to the source depth, the vertical force and horizontal tension crack Green's functions are approximately equal. We use the vertical force formulation because it is simpler

(Barker, *et. al.*, 1993). The Green's functions are discussed in the next subsection.

We model quarry blasts as the superposition of rows of charges fired in sequence, a well established paradigm (e.g., Stump and Reinke, 1988). Following the modeling studies by Barker, *et. al.*, (1993), each charge consists of an explosion with an accompanying spall, which moves material from its original location. For the explosive part, we again use the Mueller-Murphy source, and for the spall part we use a form similar to the relation for spall from a nuclear blast (above). A difference is that, for the quarry charge, the center-of-mass of the spalled material has a net displacement. Barker, *et. al* (1993) show that this has a significant effect on synthetic regional signals from quarry blasts. In this case, the dwell time is

$$t_d = \left[v_0 + \left(v_0^2 + 2z_0 g \right)^{1/2} \right] \Big/ g \ , \tag{6}$$

where z_0 is the vertical change in the center-of-mass of the spalled material. The histories from the individual charges are convolved with a temporal firing pattern for a rectangular array of charges:

$$F(\omega) = N_{cols} \sum_1^{N_{rows}} B_j e^{-i\omega t_j}$$

where N_{rows} is the number of rows of charges (rows are parallel to the quarry face), N_{cols} is the number of columns or charges per row, B_j is the source strength for each row and t_j is the firing time for the row. Here, we have assumed that the Green's functions do not vary over the quarry dimension, and that charges within a row are fired simultaneously. These assumptions are discussed in detail in Barker, *et. al.*, (1993). We have constructed a "standard" quarry blast for XNICE based on typical blasting practices. The user specifies a total yield for the blast. A burden Q of 15 meters is assumed (blasts of interest will have yields of 100 tons or more, very large blasts with large benches and burdens). We then use relations from blasting handbooks (Dupont, 1942, Langefors and Kihlstrom, 1963) for the remaining parameters:

$$dx = 1.25Q$$
$$Y_H = 0.6Q^3 \ ,$$
$$dt_f = 4x10^3 Q \ ,$$

where dx is the hole spacing, Y_H is the charge per hole (kilograms), and dt_f is the firing interval between rows. The number of holes is the total yield divided by Y_H. The blasts typically are rectangular, with the dimension parallel to the bench longer than the dimension normal to the bench. We assume that the aspect ratio is 2:1. To specify the spall parameters at each charge, we rely on observations by Langefors and Kihlstrom (1963) and set the change in center-of-mass z_0 at $Q/2$, material take-off velocity v_0 at 3.5 m/sec and the spall mass at $1.4 \times 10^4 \, Y_H$. We assume that the mean firing interval dt_f between rows is constant, as well as the mean source strength B, but each has a random variation of 20%. The source spectrum for each individual charge has an explosive part whose corner frequency is much higher than the frequencies of interest here, while the spall component peaks in the bandwidth of interest. The firing pattern spectrum $F(\omega)$ is flat at low frequencies and rolls off as f^{-1} above a corner frequency equal to the inverse of the total duration of the blast, or $N_{rows}(dt_f)^{-1}$, which for larger blasts will be around 1 Hz or less. Barker, *et. al.* (1993) show that synthetic regional signals from the explosive and spall components are comparable. The amplitudes from the quarry blast are found from

$$A_{nbex}(f, A) = \left[\hat{G}_{exp}(f) \Omega_{exp}(Y_H, f) + \hat{G}_{vf}(f) \right] F(\omega) . \tag{7}$$

The effects of the firing pattern have been observed in several regional studies (e.g., Bennett, *et. al.*, 1989; Hedlin, *et. al.*, 1990; Smith, 1988).

2.4 Source Excitation Spectra

Ideally, one would find the source excitation spectra for each source type by recording signals from the different types along common propagation paths. This is possible in many areas for quarry blasts and earthquakes, although in many areas it is not. Of course, the number of nuclear test sites is small. When these recordings are available, $E(f)$, or $\Omega(f)E(f)$ can be inferred using analyses such as in Campillo (1985). Otherwise, we must rely on synthetic seismogram calculations.

For the test cases described in Section 3, we used synthetic seismograms to compute $E(f)$ for explosion, double-couple and point-force at the required depths. We recognize that the current technology for computing synthetic seismograms is limited to plane-layered models which do not completely represent the observed wavefields. We assume, however, that spectral

differences in regional wavefields due to different sources can be predicted by the 1D synthetic calculations. The approach is to use relations derived from earthquake observations as a basis for calculating ground motions and rely on comparisons with synthetics to calculate motions from other sources with respect to earthquakes. For most regions of interest there are derived amplitude-distance formulas of the form

$$A(f_0, \Delta) = s(m_b, f_0) P_{obs}(\Delta, f_0) , \tag{8}$$

where $P_{obs}(\Delta, f)$ is as used in Equation (1). We emphasize that P is found from observations with the subscript obs. The propagation parameters γ and n and the source term $s(m_b, f)$ are found from measurements of a suite of events (Goncz, et $al.$, 1986; Herrmann, 1983). The measurements in this type of study are typically made at or near $f_0 = 1$ Hz, with the determination of $\gamma(f)$ requiring additional spectral information. There is clearly a trade-off between both source terms and the propagation term. For most regions, the majority of these events will be earthquakes, and we make the correspondence

$$s(m_b, f_0) = E_{eqk}(f_0) \Omega_{eqk}(M_0(m_b), f_0) . \tag{9}$$

Now, the synthetic Green's functions for a source type, src , can be represented in a similar way:

$$G_{src}(f, \Delta, z) = E_{src}(f, z) P_{syn}(\Delta, f), \tag{10}$$

where z is source depth, and P_{syn} is the synthetic propagation operator. Our assumption stated above that although synthetic seismograms are not absolutely correct, but relative values are correct, is roughly equivalent to assuming that the ratio

$$\frac{G_{src1}(f, \Delta, z_1)}{G_{src2}(f, \Delta, z_2)} = \frac{E_{src1}(f, z_1)}{E_{src2}(f, z_2)}$$

is accurate. Although not essential, we make a further simplifying assumption that the earthquake excitation spectrum E_{eqk} is nearly flat (Campillo, 1985 and Herrmann and Kijko, 1983). Thus, the amplitude formula for source src is given by

$$A_{src}(f, \Delta, z) = \frac{E_{src}(f, z)}{E_{eqk}(f, z)} E_{eqk}(f_0) \Omega_{src} P_{obs}(\Delta, f) . \tag{11}$$

Studies by Campillo, *et. al.* (1984) and by the authors of this report show that excitation of regional signals is nearly constant for sources within three depth regions: the very shallow crust, the mid-crust, and the lower crust. The locations of the zones vary with earth structure, but the shallow zone is where the velocities are changing rapidly with P-wave velocities less than 6 km/sec. Most earthquakes have their hypocenters in the mid-crust while man-made sources will be in the upper crust. With this in mind, we write for the excitation functions for bombs and quarry blasts:

$$A_{src}(f, \Delta, z_{sc}) = \frac{E_{src}(f, z_{sc})}{E_{eqk}(f, z_{mc})} E_{eqk}(f_0) \Omega_{src} P_{obs}(\Delta, f) .$$
(12)

Where the subscripts *sc* and *mc* indicate that the source is in shallow crust and mid-crust, respectively.

In practice, the spectral ratio is found from quotients of smoothed spectra computed by a wavenumber integration program. For the test cases discussed below, we computed Lg and Pg Green's functions at several ranges (from 400 to 800 km) and source depths (10 m, 100 m and 10 km) for a vertical force, double-couples and an isotropic source. The calculations at 10 m and 100 m are the shallow crust spectra (both depths were done as a check that the spectra were insensitive to depth within the shallow crust). The 10 km earthquake (done for 45° dip slip thrust and vertical strike slip mechanisms) was the reference mid-crustal earthquake.

2.5 Noise Models

It is essential for network performance assessment to model the effects of random processes on signals and measurements. We described above how random variations in source properties are introduced. It is not uncommon to observe signals with quite different amplitudes from closely spaced earthquakes with similar network magnitudes. Thus, SYNWAVE multiplies each computed amplitude by a random variable. For a specified value v, a computed amplitude A is replaced by

$$A \ v^{(2^*r[0,1]-1)} ,$$
(13)

where $r[0,1]$ is a uniform random variable in the domain $[0,1]$. Note that this is a relative error independent of signal strength. Typical values of v are 2 to 4, which

is equivalent to a relative m_b error of log(v), or 0.3 to 0.6, respectively. At the receiver, ground noise corrupts the signal. We model the ground noise and propagation variation separately since a criterion for detection at a site is the ratio of the signal to ground noise. Ground noise at each station is specified by a mean μ and standard deviation σ,

$$\mu + \sigma\left(2*r[0,1]-1\right) ,$$

which is added to the signal. This is an absolute error. Travel time errors are treated as absolute errors, similar to the ground noise model.

3.   Tests with Eastern and Western U.S. Structures

We have made initial tests of the XNICE regional capabilities using western and eastern U.S. structures since the elastic and anelastic structures have been extensively studied and they represent stable and tectonically active regions. We use the eastern U.S. structure found in Hermann and Kijko (1983).

Table 1. Eastern U.S. Structure					
Thickness (km)	P Velocity (km/sec)	S Velocity (km/sec)	Density (gm/cm^3)	Bulk Q	Shear Q
1	5.0	2.89	2.5	1200	600
9	6.1	3.52	2.7	1200	600
10	6.4	3.7	2.9	1200	600
20	6.7	3.87	3.0	8000	4000
20	8.15	4.7	3.4	8000	4000

In Figures 2 and 3, the normalized excitation functions (Equation 11) are shown for this structure. The results should be independent of range, so several ranges

Figure 2. Normalized *Lg* excitation functions are shown for the eastern U.S. structure. Explosion and vertical force excitation are referenced to mid-crustal double-couple.

14
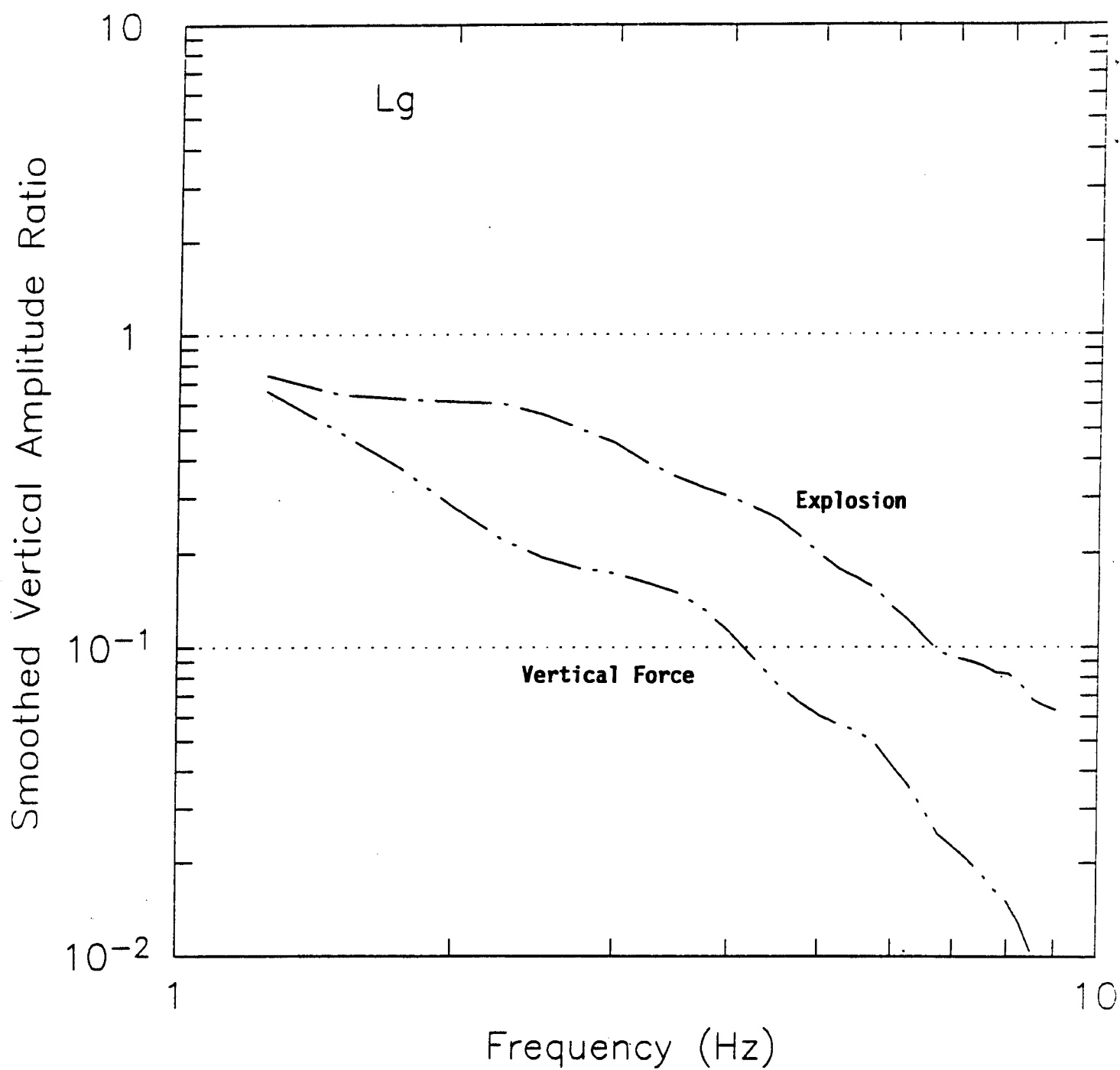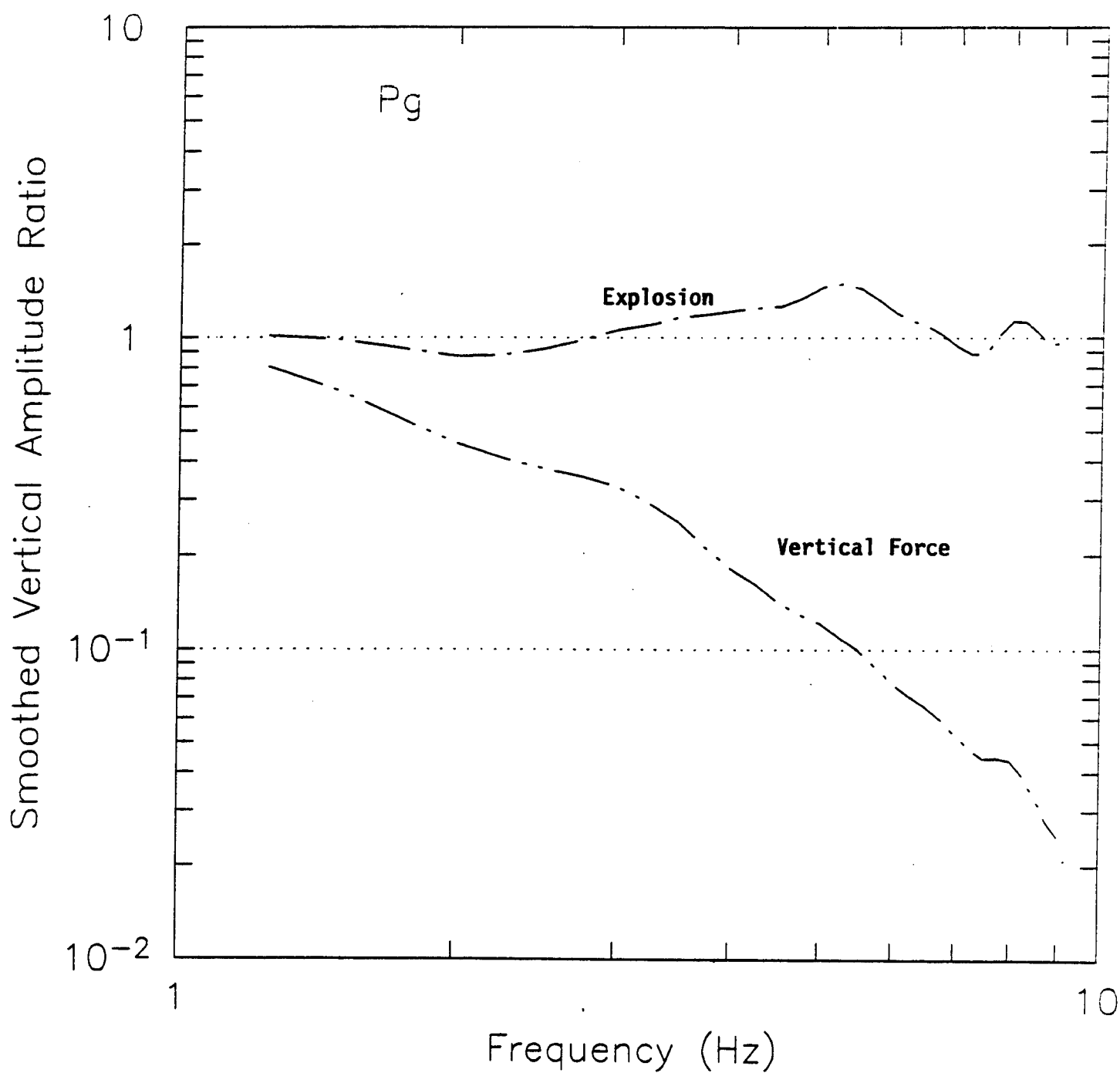
Figure 3.   Normalized *Pg* excitation functions are shown for the eastern U.S. structure. Explosion and vertical force excitation are referenced to mid-crustal double-couple.

15

were computed as a check. We see that the Lg explosion and vertical force excitation decreases with frequency relative to the mid-crustal earthquake, with the vertical force having a steeper slope. For Pg, only the relative vertical force excitation decreases with frequency. We note that the Lg explosion and earthquake excitation functions differ by only 0.28 magnitude units at 1 Hz (for constant moment rate). Previous Lg excitation studies (Swanger, *et. al.*, 1982; Bennett, *et. al.*, 1987; McLaughlin, *et. al.*, 1988) have found that there is little difference in Lg peak excitation between shallow explosion and deeper earthquake excitation. Since the peak is near 1 Hz, the results in Figure 2 are not inconsistent with their findings. In the XNICE regional propagation files, the excitation functions are parameterized as polynomials of log-frequency:

$$log \frac{E_{src}(f, z_{sc})}{E_{eqk}(f, z_{mc})} = a_0 + a_1 log(f) \, . \tag{14}$$

The values for the excitation functions shown in Figures 2 and 3 are tabulated in Table 2.

Table 2. Excitation Function Parameters Eastern U.S. Model			
Phase	**Source**	a_0	a_1
Lg	explosion vertical force	-0.28 3.3	-0.5 -1.58
Pg	explosion vertical force	-0.16 3.3	-0.10 -1.3

The EVENTS module was used to generate populations of events of the four source types. The cumulative number of earthquakes above a moment M_0 of earthquakes followed the standard distribution:

$$log(N_{cum}) = a - b \, log(M_0) \, . \tag{15}$$

For explosions and quarry blasts, the log of yield followed a uniform distribution

16

between 1 and 10 kilotons. The SYNWAVE module was used to compute amplitudes of ground motions at frequencies from 1 to 10 Hz at stations in the network.

The majority of regional discriminants proposed and tested use spectral slopes, or the ratio of an amplitude measured at low frequency to the amplitude at high frequency. The measured amplitude values are obtained by spectral averages or from narrow-band filters that are corrected for propagation and then averaged over the network. The propagation corrections are made in various ways and they are equivalent to the magnitude formulation (Herrmann and Kijko, 1983)

$$m_b = 2.94 + 0.833 \log(\Delta/10.0) + 0.4342 \gamma \Delta + \log(A_{obs}) \ . \tag{16}$$

For magnitude determination, the amplitude A_{obs} and γ are found near 1 Hz. For the amplitudes that are used to describe spectral slopes in discriminants, Equation (12) was used to make frequency-dependent distance corrections. The parameter γ is defined as

$$\gamma(f) = \frac{\pi f}{U_g Q(f)} \tag{17}$$

where U_g is the group velocity. Anelastic parameters (Table 3) in the form $Q(f) = Q_0 f^\eta$ are taken from Goncz, et. al. (1986).

Table 3. Anelastic Attenuation Parameters			
Phase	Q_0	η	U_g
Lg	1000	0.53	3500
Pg	1710	0.53	6000
Pn	825	0.80	8000

Spectral slope discriminants have been tested in several areas using the slopes of Lg and P (Pg or Pn) spectra or equivalently the ratios of amplitudes at low frequencies to amplitudes at high frequencies. Examples are Murphy and Bennett (1982), Lee, et. al. (1986), Chael (1988), Bennett, et. al. (1989), Taylor, et. al. (1989), and Hutchinson and Herrmann (1993). These studies all show that Lg and

Pg spectra from earthquakes are richer in higher frequency energy than explosions. Taylor *et. al.* (1989) also show that overburied NTS explosions have spectral slopes closer to those of earthquakes than to normally buried explosions. That is, overburied explosions are richer in high frequencies than normally buried explosions. Quarry blasts also have been shown to have steeper spectral slopes than earthquakes (Lee, *et. al.*, 1986, and Hutchinson and Herrmann, 1993).

For the eastern U.S. structure described above, we show in Figure 4 a plot of the ratio of *Lg* spectral amplitude in the band from 1 to 2 Hz to the spectral amplitude in the 6 to 8 Hz band at stations on a uniform grid (this was done to isolate the effects of source and propagation from the effects of network geometry and location uncertainties). The events are located near the center of a square grid which is 5 degrees on a side. The ratios are plotted against $m_b(Lg)$, using Equation (13). The amplitudes are computed by the SYNWAVE module (according to Equation 10) which adds station noise to the measurements. The ANALYST module finds the frequency-band averaged values at each station and computes network values, which are plotted in Figure 4. The EXAMINE module makes the plot. In this figure, the earthquake stress drop is held fixed at 100 bars to make the comparisons between source types more apparent. As can be seen in the figure (taken from the XNICE interface), the earthquakes have the lowest ratios (or the shallowest slopes). The quarry blasts have the highest *Lg* spectral ratios (steepest slopes). For lower magnitudes, the overburied bombs have ratios near those of earthquakes, but the ratios are larger for higher magnitudes. Normally buried bombs have higher ratios than earthquakes. The scatter in the normally buried bombs is due primarily to interference between the spall and explosive components at high frequencies, while the scatter in the quarry blasts is due to scalloping from the firing pattern and to low signal levels at high frequencies.

We note that a spectral slope need not be described as a ratio of amplitudes at high and low frequencies, but by a value derived from the entire spectrum. Observational studies also use a slope derived from regression. Since SYNWAVE writes the spectrum to the arrivals bulletin, we could have used this spectral measure. We chose the amplitude ratio presentation since it is more common. We shall examine the sensitivity of the discrimination results to these methodologies in the the second phase of this project.

18

75 events out of 75 from bulletin: eus.test2, network: test4.lonois
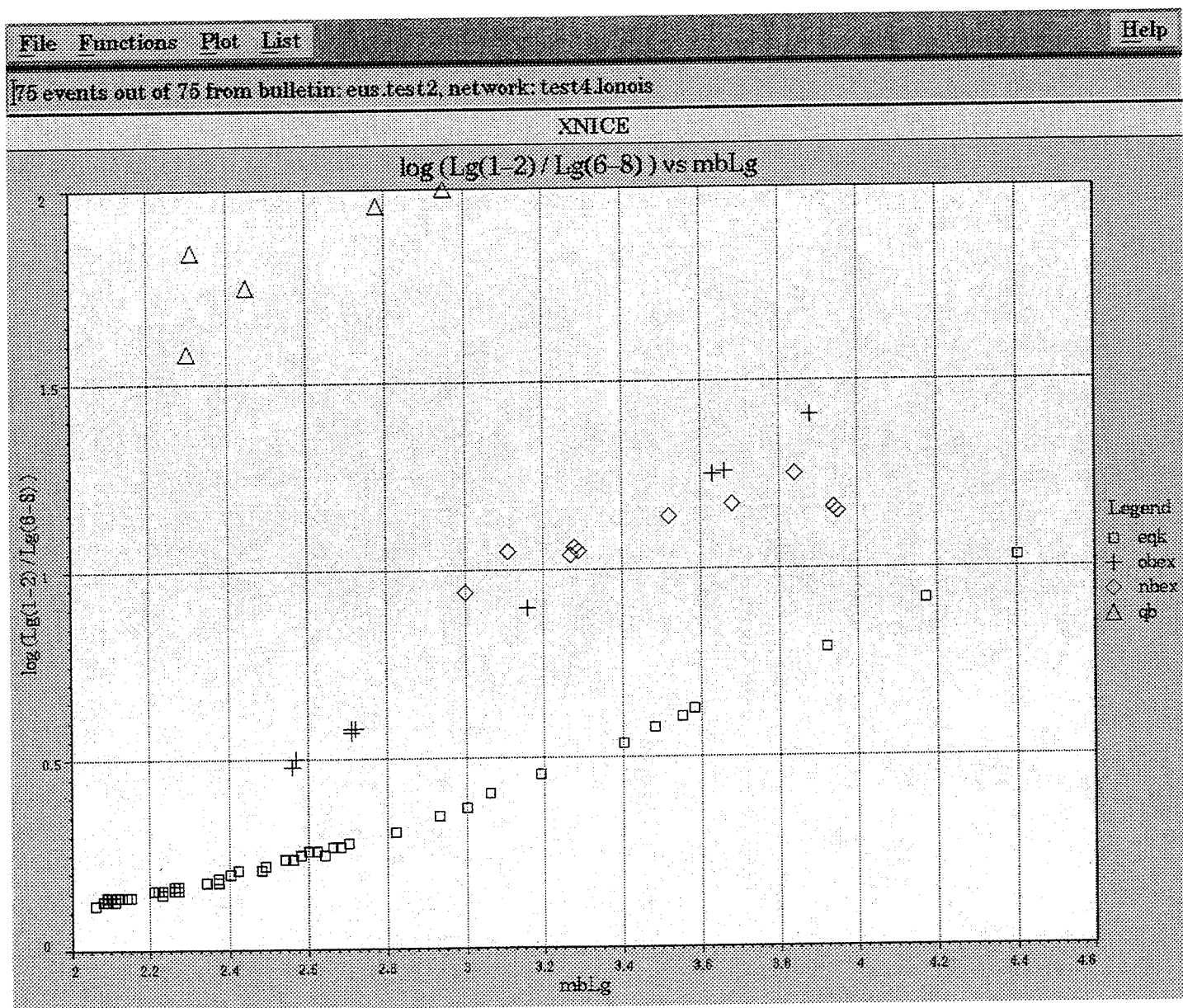
XNICE

log (Lg(1-2) / Lg(6-8)) vs mbLg

Figure 4.   Plot of the ratio of *Lg* spectral amplitude in the band from 1 to 2 Hz to the spectral amplitude in the 6 to 8 Hz band averaged over stations on a uniform grid, for the eastern U.S. structure.

19

The causes of the different slopes can be seen in Figure 5, which shows spectra of the products of the Lg excitation and source functions $E(f)\Omega(f)$ for representative sources in the 1 to 10 Hz band. The spectra have been normalized to the values at 1 Hz. The earthquake spectra, for magnitude 2.5 and 3.5 events, show the effect of decreasing corner frequency with source size. The overburied bomb has a steeper slope primarily because the explosion excitation slope relative to the earthquakes is greater (Figure 2 and Table 2). The normally buried bomb source spectrum is peaked near 1 Hz due to the spall contribution, which causes the spectral ratio to be higher for the normally buried bomb than for the overburied bomb. The quarry blast spectrum is steepest due to both the source and excitation functions. Both the shallow crust excitation functions for the explosive and spall contributions to the quarry blast decay faster than the mid-crust earthquake.

The finite duration of the quarry blast (in this case, 2.6 seconds) modulates the spectrum by a sinc function that decays as f^{-1} above about 0.4 Hz. In addition, the spall contribution is peaked below 1 Hz. The spectral ratios for the quarry blasts in Figure 4 are higher than are generally observed. A possible explanation is that although the firing intervals in the model are consistent with standard firing practices, the total durations are too long (resulting in a corner frequency which is too low). In summary, the bomb ratios separate from the earthquakes due to the relative excitation. The ratios of normally buried bombs are further increased by the spall contribution. The ratios for quarry blasts are high due to both the excitation and the source functions.

The ratio of Lg to P in different bands has also been proposed as a discriminant. Examples are Bennett, $et.\ al.$ (1989), Taylor, $et.\ al.$ (1989), Chan, $et.\ al.$ (1990), Lynnes, $et.\ al.$ (1990), Wuster (1993), and Kim, $et.\ al.$ (1994). These studies show that the ratio of Lg to Pg, and the spectral slope of Lg/Pg, are higher for both chemical and nuclear explosions than for earthquakes. Following Taylor, $et.\ al.$ (1990), we show in Figure 6

$$\log \frac{Lg/Pg(1-2\,Hz)}{Lg/Pg(6-8\,Hz)} \tag{18}$$

versus $m_b(Lg)$ for the set of sources. This rather complicated ratio is used in observational studies to minimize by cancellation the effects of propagation and enhance the effects of the source. There   is more scatter in this plot than Figure

20

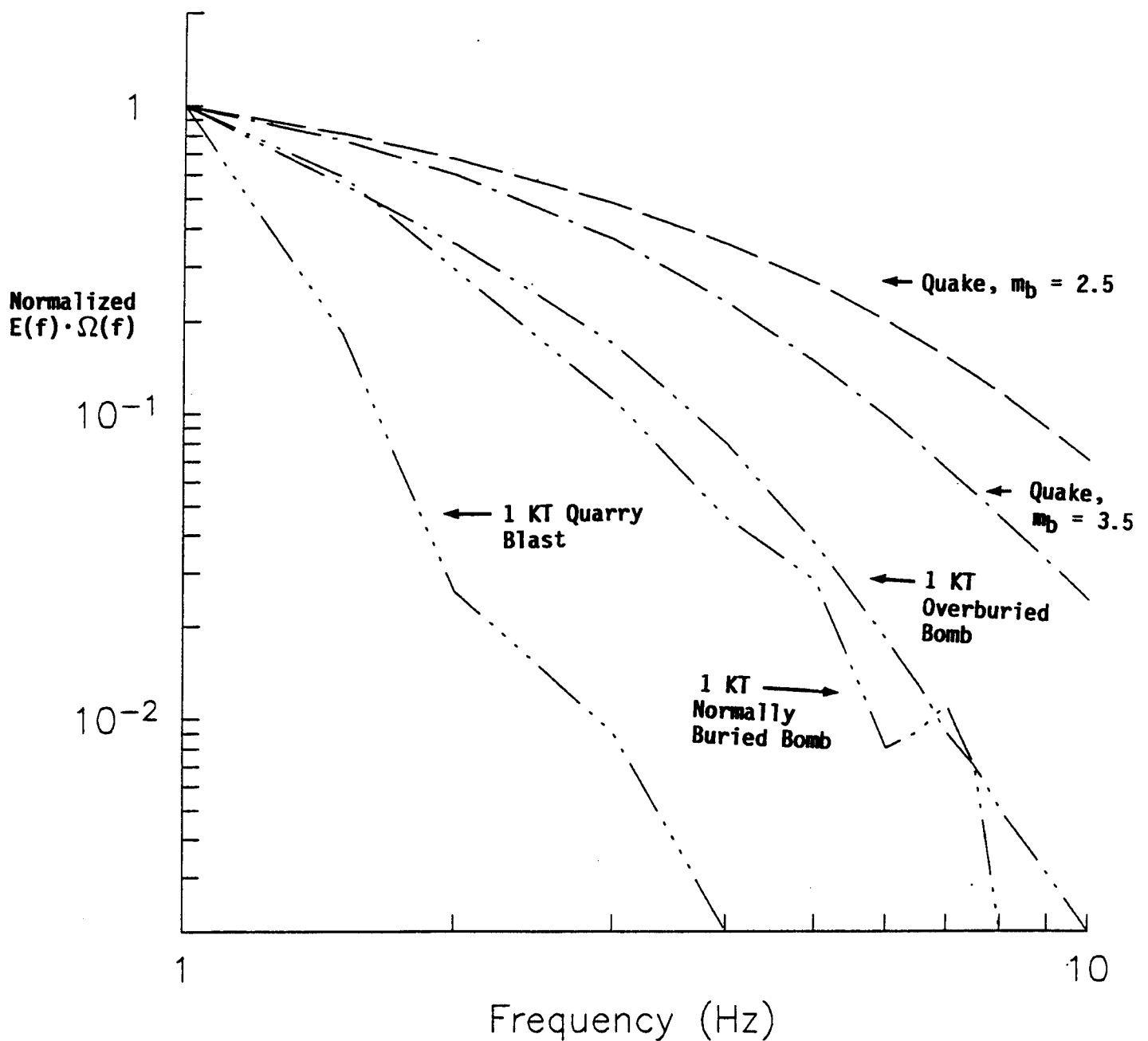Figure 5. Spectra of the products of the *Lg* excitation and source functions
$E(f) \, \Omega(f)$ for representative sources in the 1 to 10 Hz band. The
spectra have been normalized to unity at 1 Hz. Note that the quarry
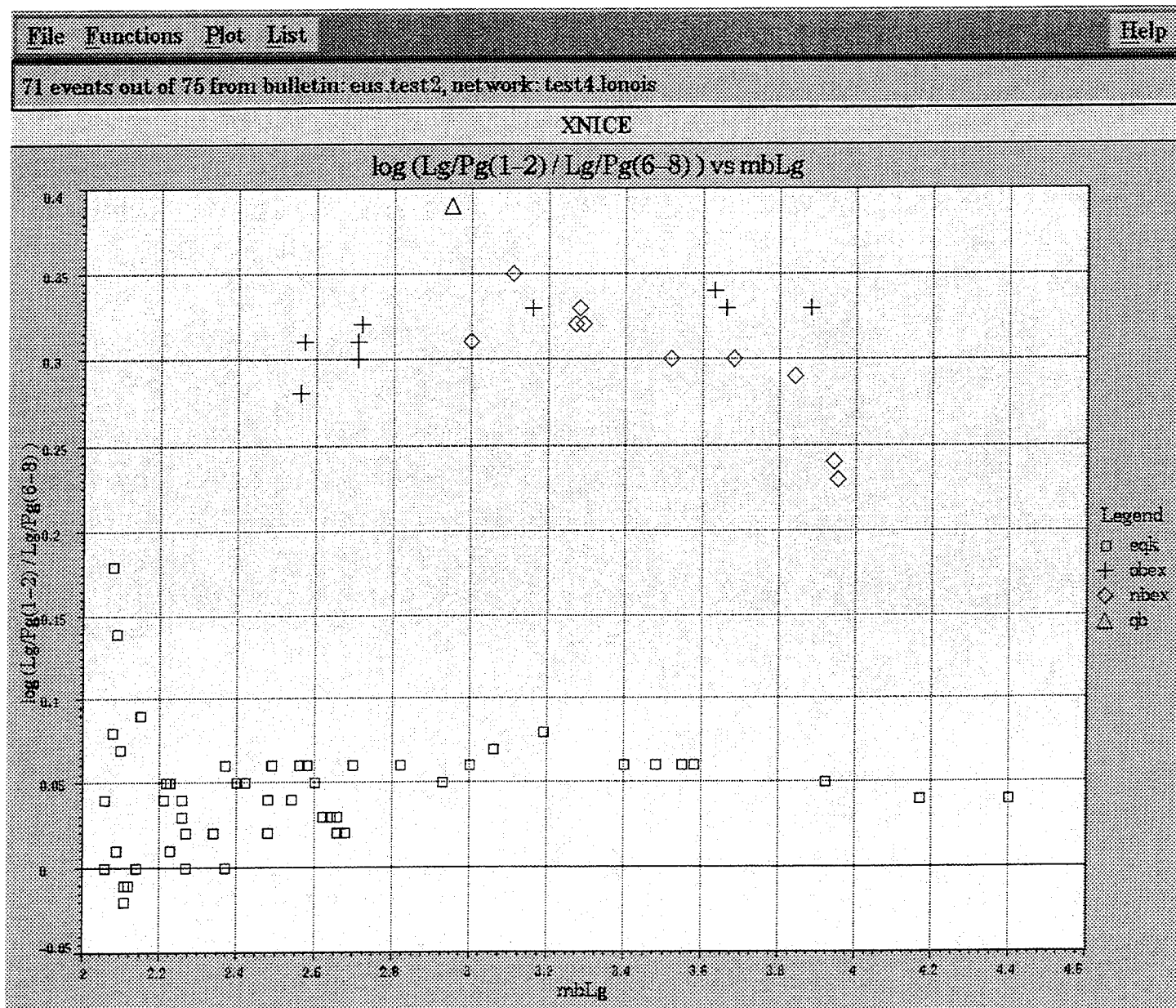blast spectrum has the steepest slopes and the earthquakes have the
shallowest slopes.

Figure 6.   Plot of

$$log \frac{Lg/Pg(1-2\,Hz)}{Lg/Pg(6-8\,Hz)}$$

for the eastern U.S. structure.

4 because the *P* wave signals are smaller than *Lg* and are more affected by station noise. Note that earthquakes have the lowest values of the ratios.

Figure 7 shows *Lg* spectral ratios for the same set of events but recorded at a simulated network of 30 U.S. National Seismograph Network (USNSN) sites. The events are located near the center of the array at 37° N by 90° W (western Tennessee). The station locations are given in Appendix A. At this time, we do not have noise data for many USNSN stations and no bulletins are yet available. Thus, we used a default value of 2 nm RMS ground noise at each site. This value is probably too low for noisy stations near the coast or populated areas and too high for remote quiet sites. For this figure, the relative random variation from propagation (Section 2.6) was not applied. The earthquake stress drops vary randomly in a uniform distribution between 80 and 120 bars. The results are similar to Figure 4 except that there is more scatter in the spectral ratios (especially at low magnitudes) and quarry blasts do not appear on the plot. The quarry blasts are not on the plot because the spectra fall off rapidly and the values at higher frequencies are below the specified signal-to-noise ratio of 2. The ANALYST module flags these as non-measurements. To further illustrate the effects of station noise, we increased the noise levels by a factor of 5 (to 10 nm), the results of which are shown in Figure 8. Note that the smaller overburied explosions do not appear on the plot because the higher frequency signals are in the noise, thus reducing the success rate of the discriminant.

In Figures 9 and 10, we show *Lg* spectral ratios for a larger suite of events in which the random variation from propagation is set at 0.2 and 0.5 magnitude units, respectively, and the station ground noise levels at 10 nm. At the higher levels, the populations of events are difficult to separate, even at high magnitudes. We note that 295 out of the 440 events in the realization are plotted. The remainder were rejected primarily because the signal-to-noise levels in the high frequency measurement were less than 2, even though the signal-to-noise levels at low frequencies were sufficient to make a magnitude measurement. Referring to the spectral slope values on the figures, we see that the level for detecting and measuring earthquake spectral slopes is around 0.2 magnitude units more than the threshold for making a magnitude measurement. Since the spectral slope of the artificial sources is higher than for earthquakes, the threshold for measuring the spectral slope is even higher for these sources, about 1 magnitude unit.

23

Figure 7.   Plot of the ratio of *Lg* spectral amplitude in the band from 1 to 2 Hz to the spectral amplitude in the 6 to 8 Hz band averaged over stations in the USNSN for the eastern U.S. structure. No random propagation variation is included.

24

70 events from bulletin: eus.test4, network: nsn.30

XNICE

log (Lg(1-2) / Lg(6-8)) vs mbLg

Figure 8.   Plot of the ratio of *Lg* spectral amplitude in the band from 1 to 2 Hz
to the spectral amplitude in the 6 to 8 Hz band averaged over
stations in the USNSN with ground noise equal to 10 nm, for the
eastern U.S. structure. No random propagation variation is
included.

XNICE

Figure 9.   Plot of the ratio of *Lg* spectral amplitude in the band from 1 to 2 Hz to the spectral amplitude in the 6 to 8 Hz band averaged over stations in the USNSN with noise equal to 10 nm, for the eastern U.S. structure. The random propagation variation is 0.2 magnitude units.
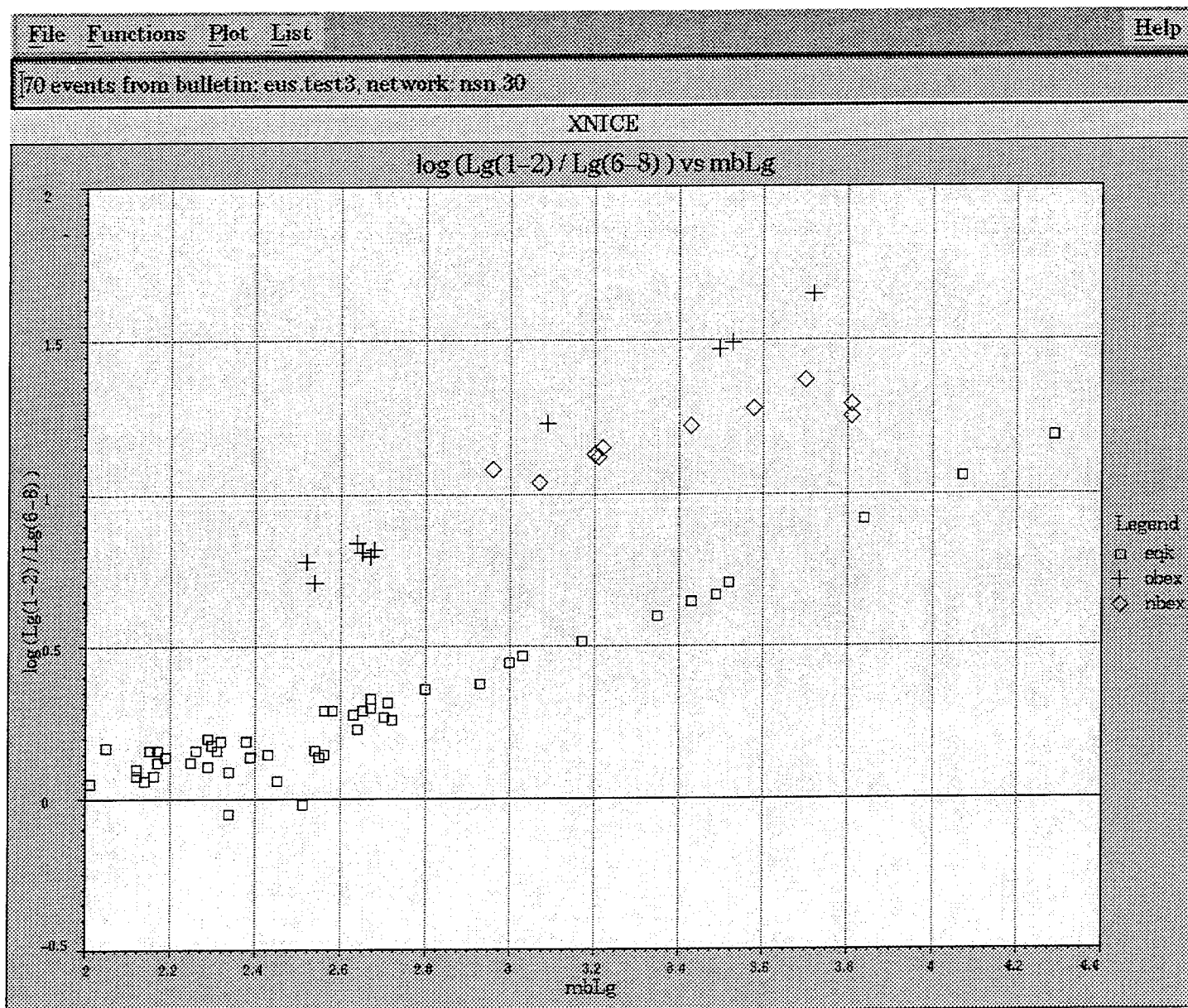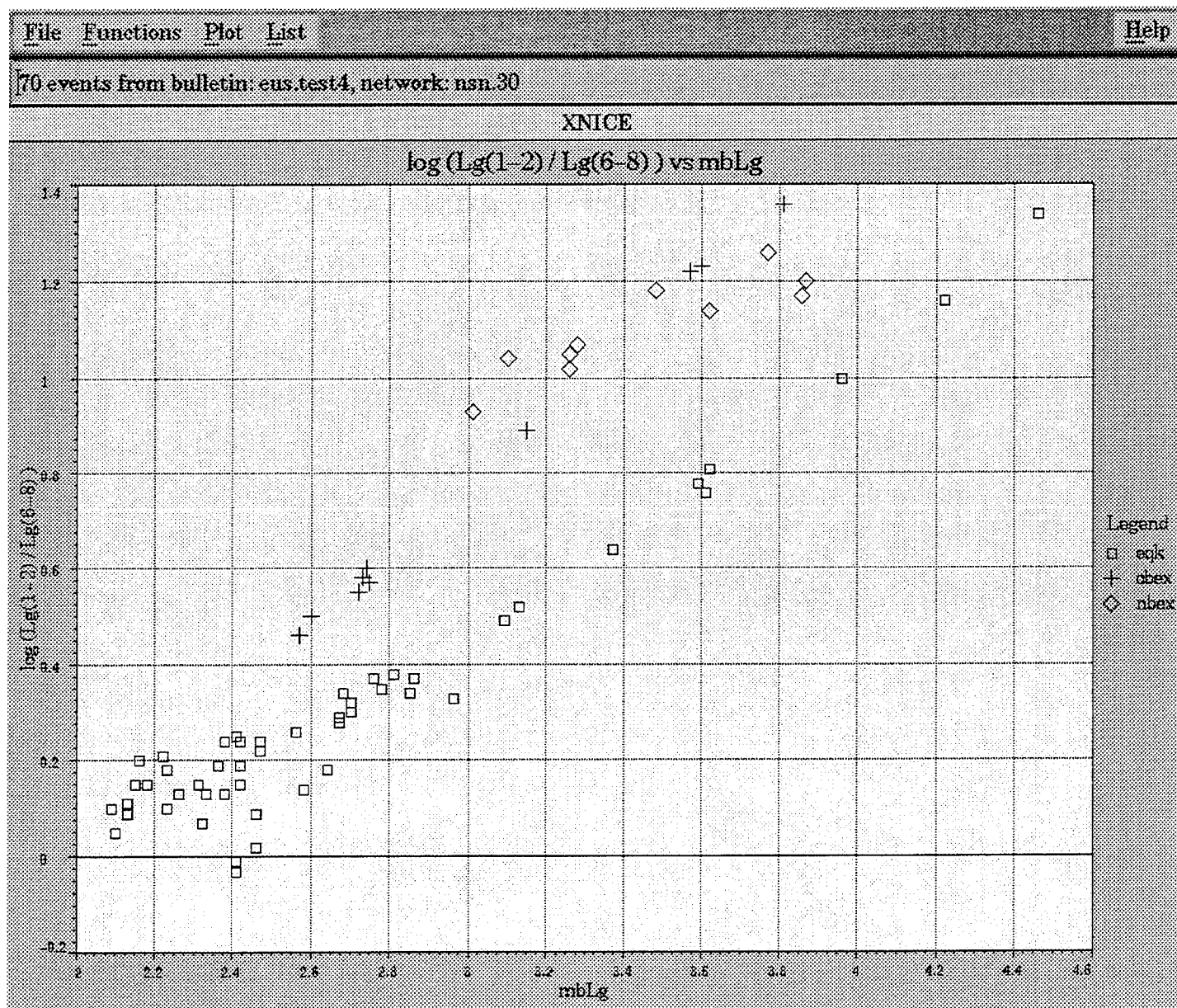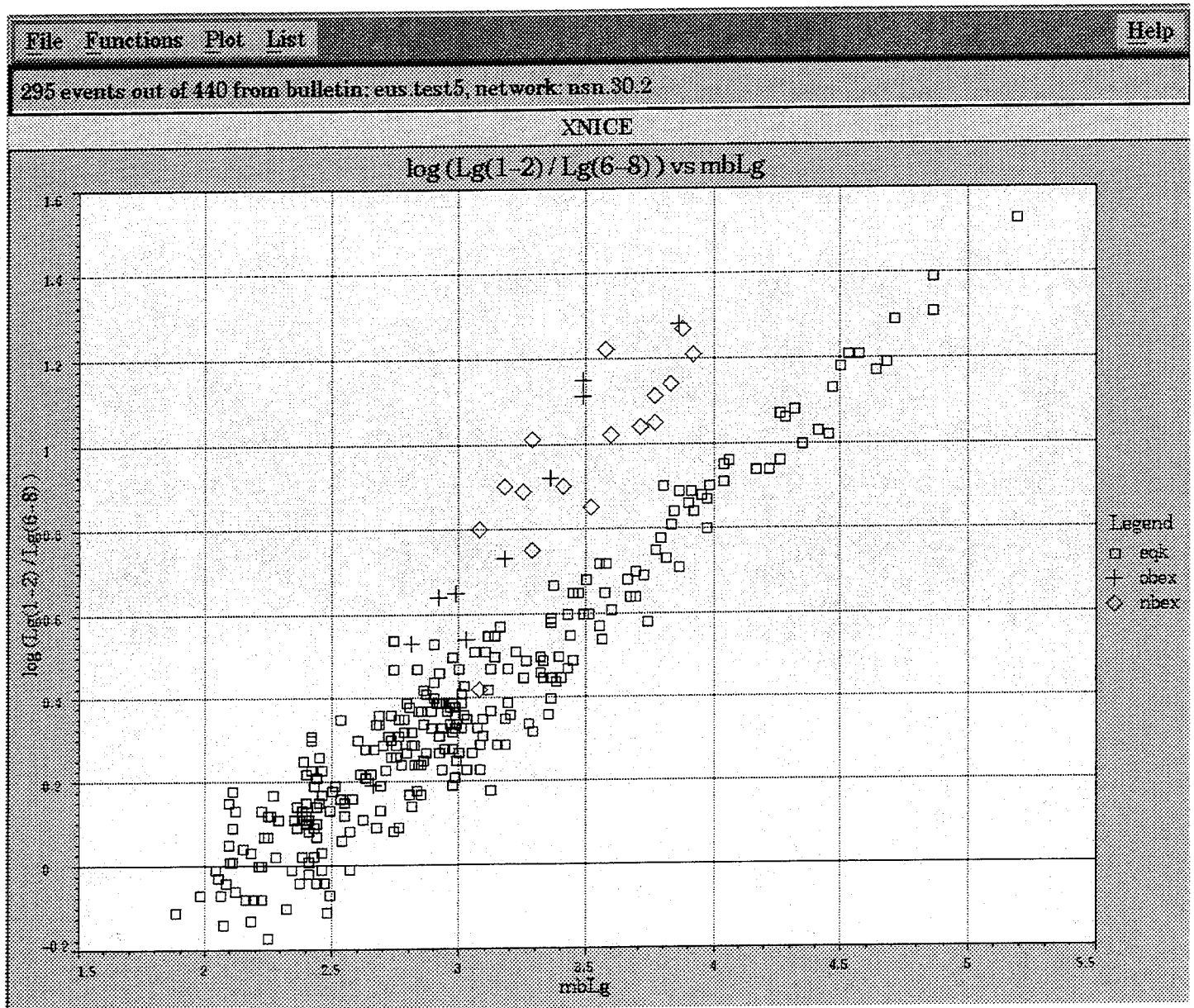
Figure 10. Plot of the ratio of *Lg* spectral amplitude in the band from 1 to 2 Hz to the spectral amplitude in the 6 to 8 Hz band averaged over stations in the USNSN with noise equal to 10 nm, for the eastern U.S. structure. The random propagation variation is 0.5 magnitude units.
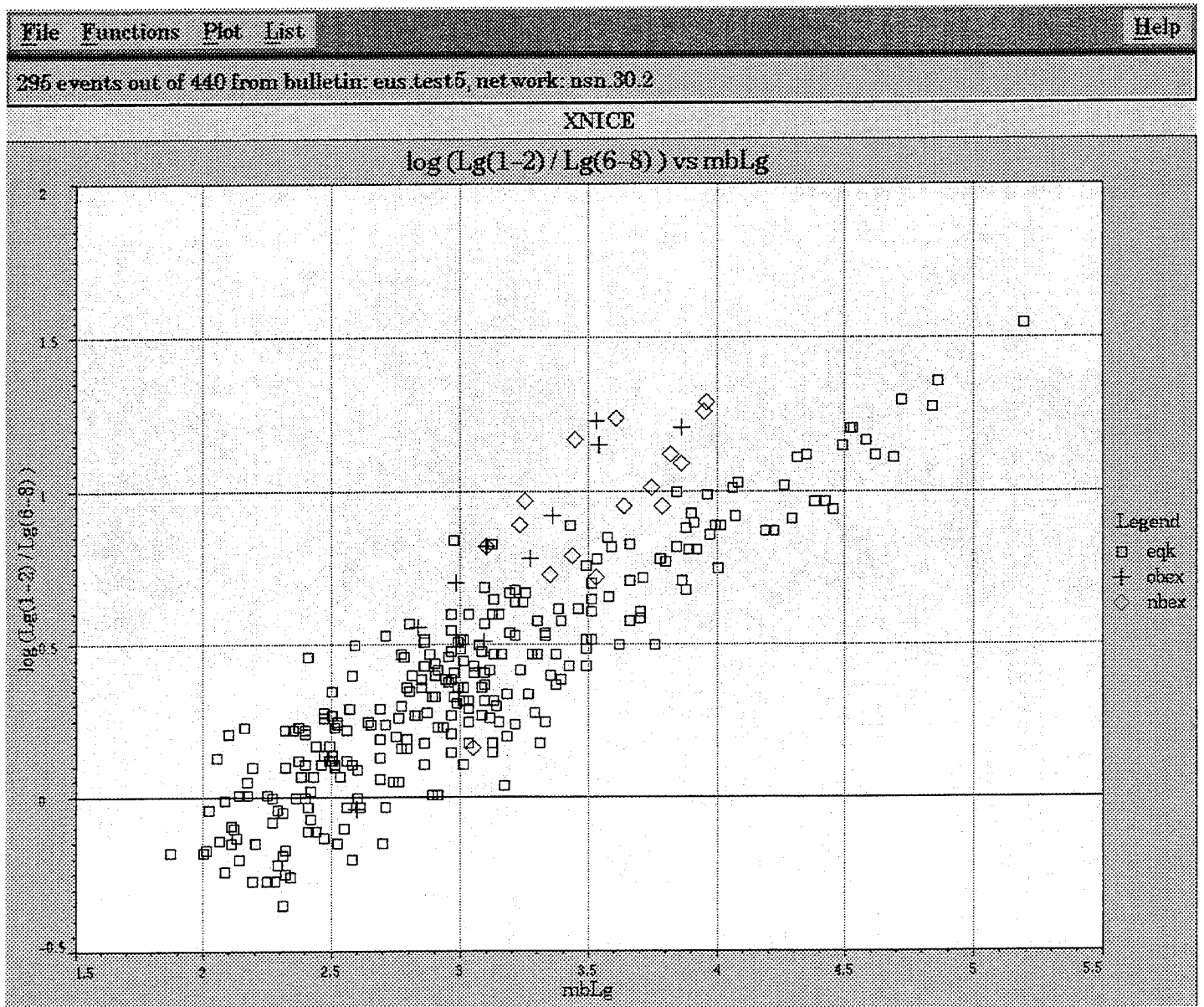
27

Our results qualitatively support the use of *Lg* and *Lg/Pg* spectral ratios as a regional discriminant, but demonstrate the sensitivity of this discriminant to network detection thresholds.

Spectral ratios computed in a network are strongly influenced by the detection levels within the network. We show in Figures 11 to 13 the predicted earthquake detection levels and location uncertainties for the simulated USNSN as functions of source locations in the eastern U.S as computed by XNICE. The network in Appendix A has been augmented by proposed stations (those with "nsn" station names). Figure 11 shows contours of RMS error in locating a magnitude 3.5 earthquake using teleseismic (*P* and *pP*) and regional (*Pn* and *Lg*) phases. For this calculation, random travel time errors were given 1 sec RMS error for teleseismic phases, 2.5 sec error for *Pn* and 5 sec error for *Lg*. The contours are controlled by the station geometry and the number of signals which can be detected at each station. A detection is a signal whose amplitude is two times the RMS noise. Contours of the number of stations detecting *Lg* and *Pn* signals are shown in Figures 12 and 13. As expected, more stations detect *Lg* than *Pn*.

We have performed similar tests using a western U.S. model from McLaughlin, *et. al.* (1988), given in Table 4.

Note that the slopes of the excitation functions for the western U.S. are somewhat different than for the east (Table 2). The performance of the *Lg* spectral ratio discriminant is shown in Figure 14. The population of ratios of normally buried explosions do not separate from the earthquakes as much as for the eastern U.S. model, and the normally buried explosion population is mixed with the earthquakes. This is consistent with results from Taylor, *et. al.*, (1990) for NTS overburied explosions and western U.S. earthquakes. The quarry blasts are still quite distinct.
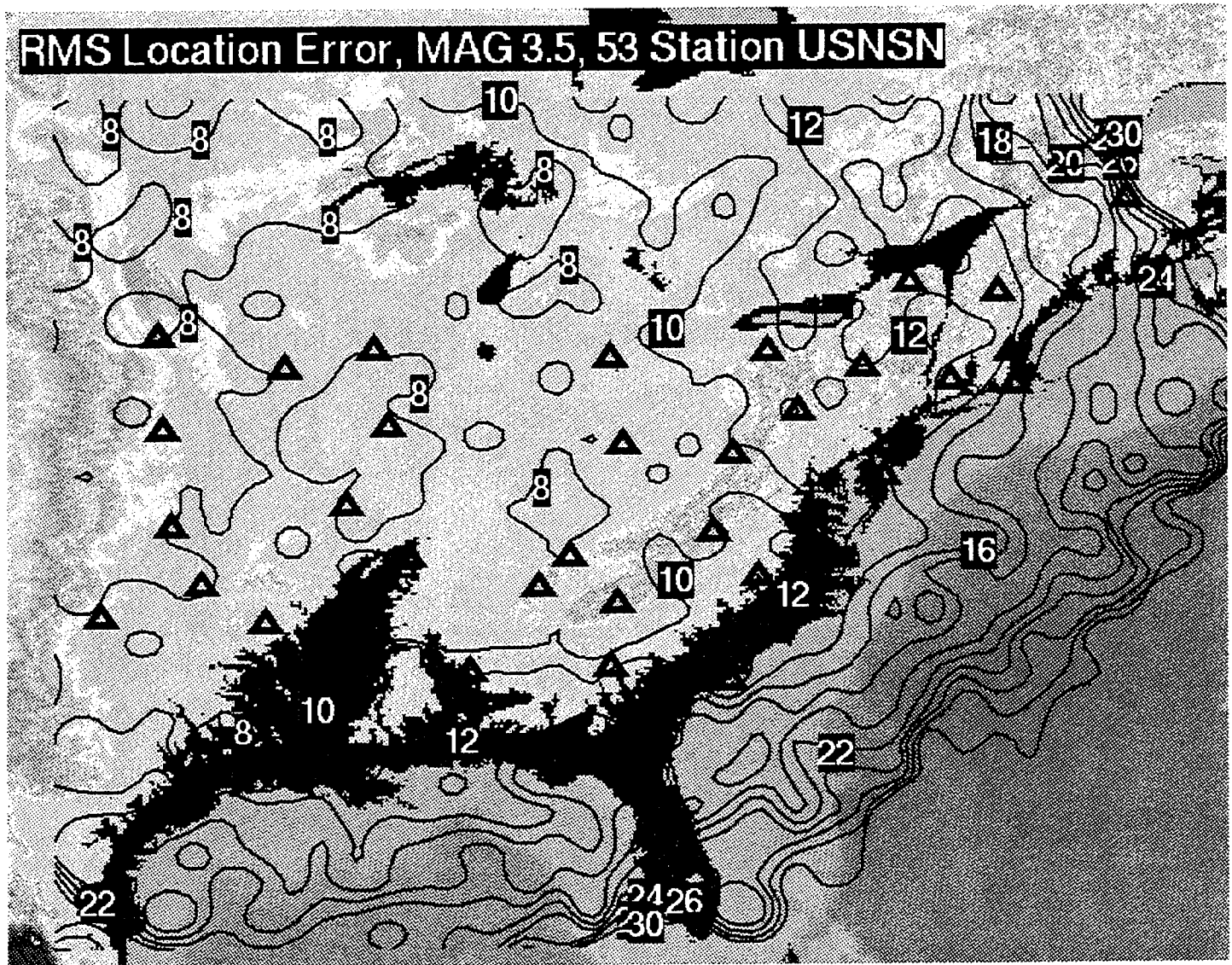
Figure 11.   RMS earthquake location error (km) contoured for an earthquake of
depth 10 km and magnitude 3.5, recorded on a simulated network
of 53 existing and proposed USNSN stations (triangles).
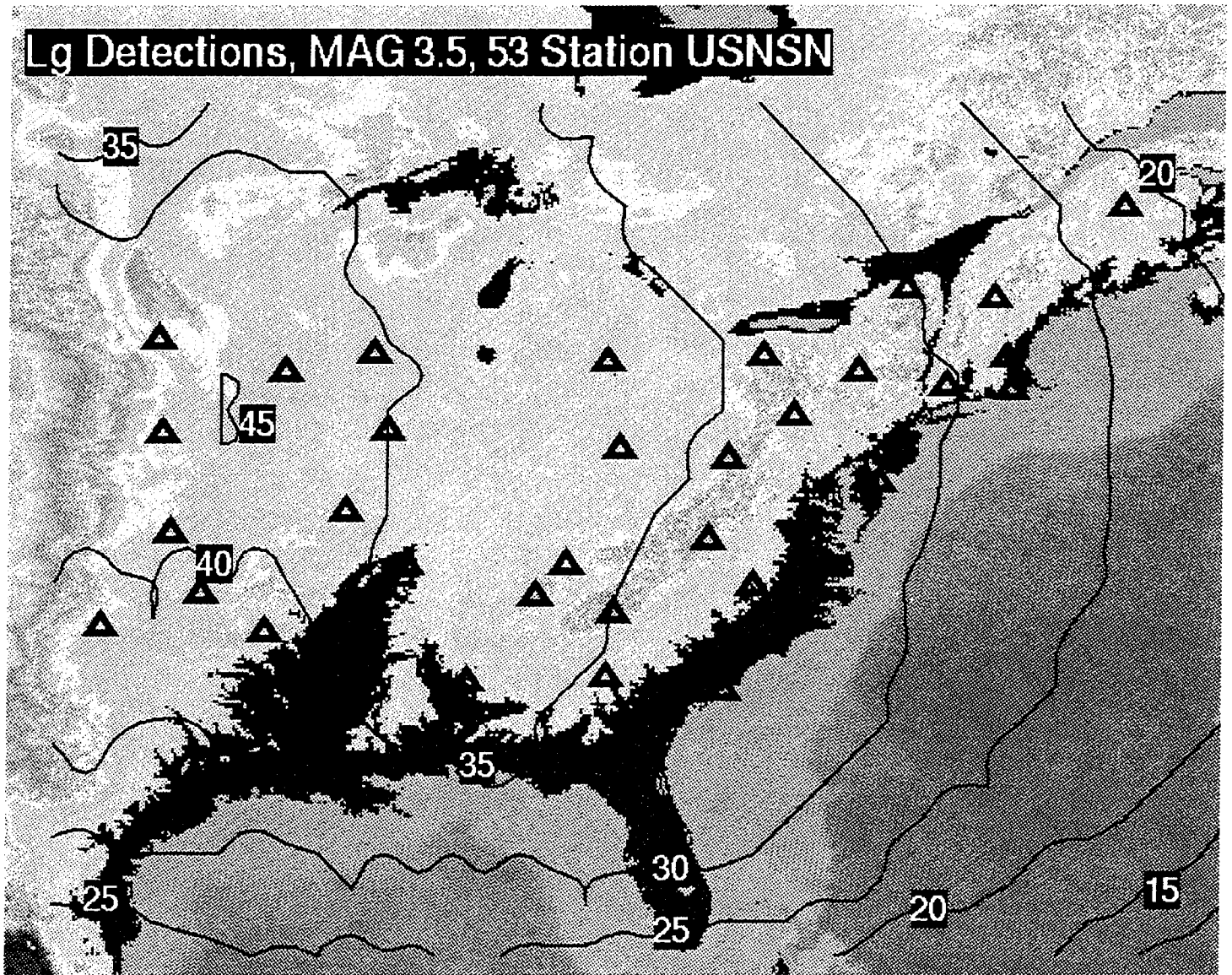
Figure 12.   Number of 1 Hz *Lg* detections is contoured for an earthquake of depth 10 km and magnitude 3.5, recorded on a simulated network of 53 existing and proposed USNSN stations (triangles).
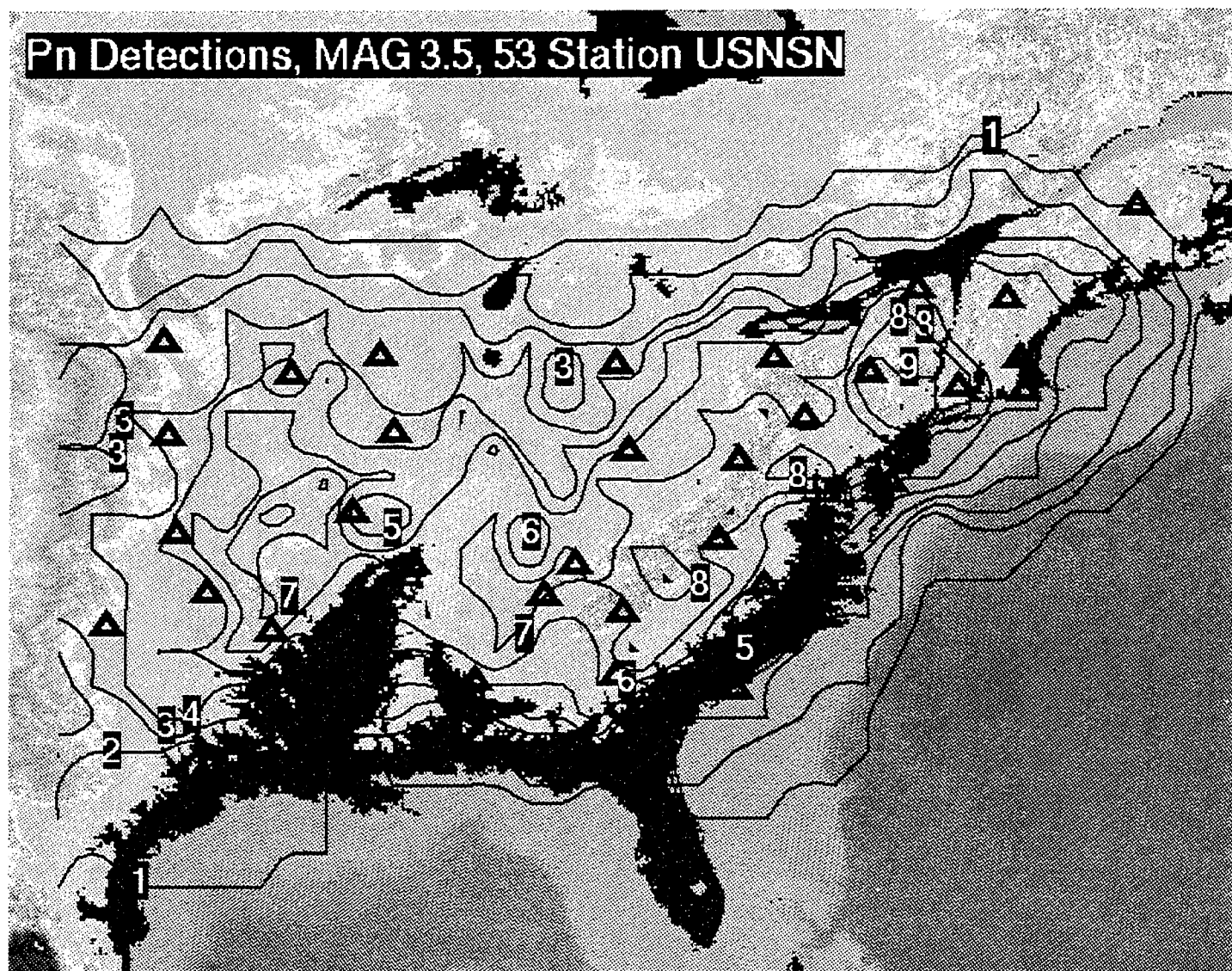
Figure 13. Number of 1 Hz *Pn* detections is contoured for an earthquake of depth 10 km and magnitude 3.5, recorded on a simulated network of 53 existing and proposed USNSN stations (triangles).

31

74 events out of 75 from bulletin: wus.test2, network: test3.lonois

XNICE

log (Lg(1–2) / Lg(6–8)) vs mbLg
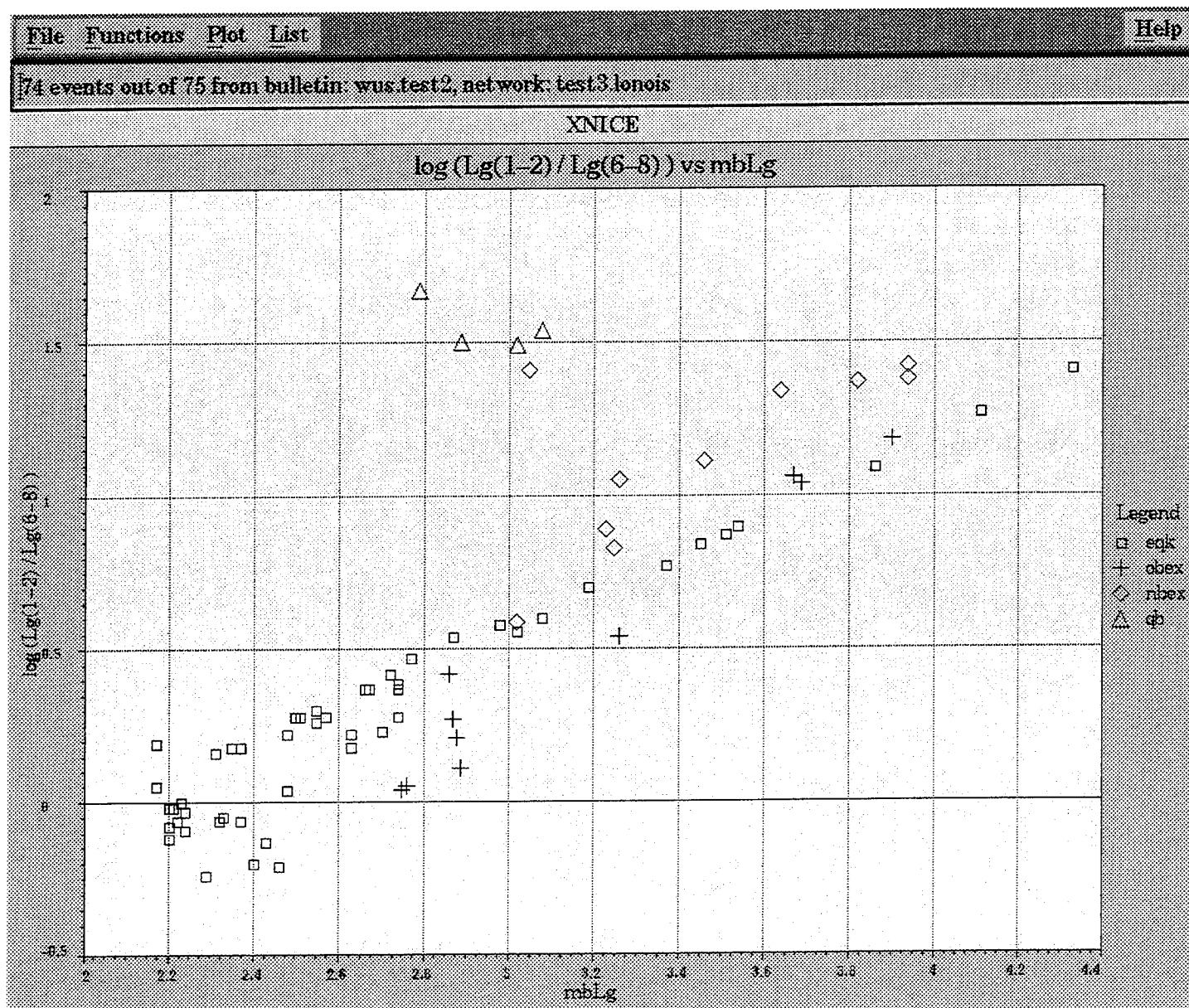
Figure 14.   Plot of the network averaged ratio of *Lg* spectral amplitude in the band from 1 to 2 Hz to the spectral amplitude in the 6 to 8 Hz band for the western U.S. structure.

Table 4. Western U.S. Structure					
Thickness (km)	P Velocity (km/sec)	S velocity (km/sec)	Density (gm/cm^3)	Q_P	Q_S
0.122	1.208	0.664	1.60	150	75
0.460	2.025	1.109	1.95	150	75
1.318	2.887	1.581	2.0	200	100
0.5	3.4	2.2	2.2	200	100
0.5	3.8	2.2	2.2	200	125
0.5	4.8	2.8	2.6	250	125
1	5.8	3.4	2.8	250	125
3	6.0	3.46	2.9	250	125
12	6.3	3.64	2.9	300	150
4	6.5	3.75	2.9	300	150
4	6.8	3.93	3.0	300	150
6	6.9	3.98	3.0	300	150
4	7.8	4.5	3.2	400	200
4	7.84	4.5	3.2	400	200
4	7.88	4.5	3.2	400	200
4	7.92	4.5	3.2	400	200
4	7.96	4.5	3.2	400	200
4	8.0	4.5	3.2	400	200
2	7.95	4.5	3.2	400	200
10	7.9	4.4	3.2	150	75
10	7.8	4.2	3.2	150	75
20	7.8	4.2	3.2	150	75
20	7.9	4.5	3.2	150	75
60	8.0	4.55	3.3	150	75
20	8.1	4.6	3.4	300	150

The excitation function parameters for this model are in Table 5.

Table 5. Excitation Function Parameters Western U.S. Model			
Phase	Source	a_0	a_1
Lg	explosion	-0.12	-1.1
	vertical force	3.1	-1.2
Pg	explosion	-0.2	-0.10
	vertical force	3.0	-1.5

4. Summary and Research Plans for the Second Year

This report describes the XNICE program, focusing on enhancements for regional discrimination of earthquakes from several artificial sources. We present a model for simulating the spectral slope discriminants, and test it using earth models for the eastern and western U.S. The model explicitly includes the effects of source spectrum and excitation on observed spectral amplitudes. For these tests, we calibrated the source excitation functions using spectral ratios of synthetic Green's functions. For populations of earthquakes, normally buried and overburied explosions and quarry blasts, we find that the relative values of spectral slopes (ratios of high to low frequency amplitudes) are consistent with observations of those source types at regional distances. We recognize that these results depend strongly on the relative slopes of the source spectra and excitation functions, which in turn depend on the earth structure. It is therefore important to test the model in different areas where there have been earth structure and discrimination studies, in particular, Europe. This will be a subject of research in the second year of this project.

The models described in this report predict that spectral slopes for Lg, Pg and Lg/Pg are least for earthquakes, are greater for normally buried explosions and are greatest for quarry blasts. Spectral slopes of Lg are closer to earthquakes for overburied bombs, and can be indistinguishable at low magnitudes. Spectral slopes are higher for normally buried bombs than for earthquakes due to the slope of (1) the spall source spectrum and (2) of the excitation spectrum of shallow explosions relative to mid-crustal earthquakes. Quarry blast spectral slopes are largest due to the effects of spall and of extended source duration. These results are all consistent with numerous observations. Furthermore, we find that the population of spectral slopes of normally buried explosions separate from earthquakes more for an eastern U.S. earth structure than for the western structure. We also show that network detection levels strongly influence these results. In particular, the identification thresholds for spectral slope methods are 0.2 to 1.0 magnitude units higher than the threshold for measuring magnitude. This is because the higher frequency energy is comparable to ground noise for small events.

We have completed most of the programming to test three other proposed regional discriminants : (1) Rg spectral slopes, (2) Rg to Lg ratios, and (3) $M_0{:}m_b$.

These will be fully implemented in the first and second quarter of the second year.

Another enhancement which we will soon test is the effects of arrays on network performance. The focus will be on improvements in event location using azimuth and slowness information from array(s) and on the effects of improved detection levels due to the array(s).

When these improvements have tested, we will apply the system to likely scenarios in the Middle East.

5. References

Barker, T.G., K.L. McLaughlin and J. L. Stevens (1993), "Numerical Simulation of Quarry Blast Sources," Phillips Laboratory, Albuquerque SSS-TR-93-13859.

Bennett, T. J., B. W. Barker and K.L. McLaughlin and J. R. Murphy (1989), "Regional Discrimination of Quarry Blasts, Earthquakes and Underground Nuclear Explosions," Air Force Geophysics Laboratory GL-TR-89-0114, ADA223148.

Bouchon, M., M. Campillo, St. Gaffet, B. Massignon, P. Mechler and F. Riviere (1991), "Propagation of Regional Seismic Phases in Western Europe," Radiomana-Societe Civile, Phillips Laboratory PL-TR-91-2064, ADA237622.

Campillo, M., M. Bouchon and B. Massinon (1984), "Theoretical Study of the Excitation, Spectral Characteristics and Geometrical Attenuation of Regional Phases," *Bull. Seism. Soc. Am., 74(1)*, pp. 179-90.

Campillo, M., J.-L. Plantet, and M. Bouchon (1985), "Frequency-Dependent Attenuation in the Crust Beneath Central France from *Lg* Waves: Data Analysis and Numerical Modeling" *Bull. Seism. Soc. Am., 75(5)*, pp. 1395-1411.

Chael, E. P., "Spectral Discrimination of NTS Explosions and Earthquakes in the Southwestern United States Using High-Frequency Regional Data," *Geophys. Res. Lett., 15(6)*, pp. 625-628.

Chan, W. W., R. Baumstark and R. K. Cessaro (1990), "Spectral Discrimination Between Explosions and Earthquakes in Central Eurasia," Air Force Geophysics Laboratory, GL-TR-90-0217, ADA230048.

Day, S. M. and K.L. McLaughlin (1991), "Seismic Source Representations for Spall," *Bull. Seism. Soc. Am., 81*, pp. 191-201.

Hedlin, M. A. H., J. B. Minster and J. A. Orcutt (1990), "An Automatic Means to Discriminate Between Earthquakes and Quarry Blasts," *Bull. Seism. Soc. Am.,*

80(6), pp. 2143-2160.

Herrmann R. B. and A. Kijko (1983), "Short-Period *Lg* Magnitudes: Instrument, Attenuation and Source Effects," *Bull. Seism. Soc. Am., 73(6),* pp. 1835-1850

Hutchenson, K. D. and R. B. Herrmann (1993), "Spectral Examination of the 16 June 1992 Earthquake and Quarry Blast Near Evansville, Indiana," *Seism. Res. Lett., 64(2),* pp 169-185.

Kim, W.-Y., D. W. Simpson and P. G. Richards (1993), "Discrimination of Earthquakes and Explosions in Eastern United States Using Regional High-Frequency Data," *Geophys. Res. Lett., 20(14),* pp. 1507-1510.

Kim., W. Y., D. W. Simpson and P. G. Richards (1994), "High-Frequency Spectra of Regional Phases from Earthquakes and Chemical Explosions," in press, *Bull. Seism. Soc. Am.*

Lee, W. H. K. (1986), "Investigation of Signal Characteristics of Quarry Blasts, Nuclear Explosions and Shallow Earthquakes for Regional Discrimination Purposes," USGS Quarterly Report to ARPA, April-June.

Lynnes, C. S., R. Baumstark, R. K. Cessaro and W. W. Chan (1990), "*Pg/Lg* Discrimination in the Western United States" Teledyne Geotech Report to Air Force Geophysics Laboratory, GL-TR-90-0167, ADA226819.

McLaughlin, K. L., T. G. Barker, S. M. Day, B. Shkoller and J. L. Stevens (1988), "Effects of Depth of Burial and Tectonic Strain Release on Regional and Teleseismic Waveforms," Air Force Geophysics Laboratory, AFGL-TR-88-0314, ADA207541.

Murphy, J. R. and T. J. Bennett (1982), "A Discrimination Analysis of Short-Period Regional Seismic Data Recorded at Tonto Forest Observatory," *Bull. Seism. Soc. Am., 72(4),* pp. 1351-1366.

Patton, H. J., "Characterization of Spall from Observed Strong Ground Motions on Pahute Mesa," *Bull. Seism. Soc. Am., 80(5),* pp. 1326-1345.

Patton, H. J. and S. R. Taylor (1993), "Analysis of *Lg* Spectral Ratios from NTS Explosions: Implications for the Source Mechanisms of Spall and the Generation of *Lg* Waves," submitted to *Bull. Seism. Soc. Am.*

Smith, A. T. (1988), "High-frequency Seismic Observations and Models of Chemical Explosions: Implications for Discrimination of Ripple-Fired Mining Blasts," *Bull. Seism. Soc. Am., 79,* pp. 1089-1010.

Street, R. L., R. B. Herrmann and O. W. Nuttli (1975), "Spectral Characteristics of the *Lg* Wave Generated from Central United States Earthquakes," *Bull. Seism. Soc. Am., 41,* pp. 51-63.

Stump, B. W. and R. E. Reinke (1988), "Experimental Confirmation of Superposition from Small-Scale Explosions," *Bull. Seism. Soc. Am., 78*, pp. 1059-1073

Taylor, S. R., N. W. Sherman, M. D. Denny (1988), "Spectral Discrimination Between NTS Explosions and Western United States Earthquakes at Regional Distances," *Bull. Seism. Soc. Am., 78(4)*, pp. 1563-1579.

Taylor, S. R., M. D. Denny, E. S. Vergino and R. E. Glaser (1989), "Regional Discrimination Between NTS Explosions and Western United States Earthquakes," *Bull. Seism. Soc. Am., 79(4)*, pp. 1142-1176.

Woods, B. B., S. Kedar and D. V. Helmberger, "M_L:M_0 as a Regional Discriminant," *Bull. Seism. Soc. Am., 83(4)*, pp. 1167-1183.

Wuster, J. (1993), "Discrimination of Chemical Explosions and Earthquakes in Central Europe - A Case Study," *Bull. Seism. Soc. Am., 83(4)*, pp. 1184-1212.

Appendix A.

The National Seismograph Network station locations used for this report are given in this table.

Table A1. Existing NSN Stations		
Station Name	**North Latitude**	**West Longitude**
ALQ	34.9425	106.4575
BDW	42.7761	109.5682
BLA	37.2113	80.4210
BMN	40.4314	117.2217
CBM	46.9325	68.1208
CEH	35.8908	79.0927
CMB	38.0350	120.3848
COL	64.9000	147.7933
COR	44.5857	123.3031
DUG	40.1950	112.8133
ELK	40.7448	115.2387
GOL	39.7002	105.3711
HRV	42.5072	71.5625
ISA	35.6633	118.4733
KIP	21.4233	158.0149
KNB	37.0166	112.8224
LTX	29.3338	103.6668
MNV	38.4322	118.1543
NEW	48.2633	117.1200
RSCP	35.5999	85.5688
RSNY	44.5483	74.5300
RSSD	44.1204	104.0361
SCP	40.7950	77.8650
TUC	32.3097	110.7822
WDC	40.5800	122.5397
CCM	38.0556	91.2446
MZ-AR	34.5586	93.6577
BNY	42.0895	75.9708
LS-NH	44.2383	71.9225
WMO	34.7138	98.5909

Table A2. Proposed NSN Stations		
Station Name	North Latitude	West Longitude
nsn15	41.53	71.44
nsn16	41.66	73.36
nsn17	38.87	75.35
nsn18	39.54	79.84
nsn19	32.84	79.93
nsn20	35.09	83.25
nsn21	33.22	83.46
nsn22	36.54	84.63
nsn23	33.09	87.62
nsn24	30.31	95.73
nsn25	35.34	90.61
nsn26	35.67	95.60
nsn27	37.42	96.52
nsn28	40.29	96.77
nsn29	43.03	96.89
nsn30	42.07	93.11
nsn31	36.50	89.45
nsn32	40.40	90.03
nsn33	39.83	83.05
nsn34	42.65	90.41
nsn35	42.40	83.46
nsn36	42.53	78.80

Prof. Thomas Ahrens
Seismological Lab, 252-21
Division of Geological & Planetary Sciences
California Institute of Technology
Pasadena, CA 91125

Prof. Keiiti Aki
Center for Earth Sciences
University of Southern California
University Park
Los Angeles, CA 90089-0741

Prof. Shelton Alexander
Geosciences Department
403 Deike Building
The Pennsylvania State University
University Park, PA 16802

Dr. Thomas C. Bache, Jr.
Science Applications Int'l Corp.
10260 Campus Point Drive
San Diego, CA 92121 (2 copies)

Prof. Muawia Barazangi
Cornell University
Institute for the Study of the Continent
3126 SNEE Hall
Ithaca, NY 14853

Dr. Douglas R. Baumgardt
ENSCO, Inc
5400 Port Royal Road
Springfield, VA 22151-2388

Dr. T.J. Bennett
S-CUBED
A Division of Maxwell Laboratories
11800 Sunrise Valley Drive, Suite 1212
Reston, VA 22091

Dr. Robert Blandford
AFTAC/TT, Center for Seismic Studies
1300 North 17th Street
Suite 1450
Arlington, VA 22209-2308

Dr. Steven Bratt
ARPA/NMRO
3701 North Fairfax Drive
Arlington, VA 22203-1714

Dale Breding
U.S. Department of Energy
Recipient, IS-20, GA-033
Office of Arms Control
Washington, DC 20585

Dr. Jerry Carter
Center for Seismic Studies
1300 North 17th Street
Suite 1450
Arlington, VA 22209-2308

Mr Robert Cockerham
Arms Control & Disarmament Agency
320 21st Street North West
Room 5741
Washington, DC 20451,

Dr. Zoltan Der
ENSCO, Inc.
5400 Port Royal Road
Springfield, VA 22151-2388

Dr. Stanley K. Dickinson
AFOSR/NM
110 Duncan Avenue
Suite B115
Bolling AFB, DC

Dr Petr Firbas
Institute of Physics of the Earth
Masaryk University Brno
Jecna 29a
612 46 Brno, Czech Republic

Dr. Mark D. Fisk
Mission Research Corporation
735 State Street
P.O. Drawer 719
Santa Barbara, CA 93102

Dr. Cliff Frolich
Institute of Geophysics
8701 North Mopac
Austin, TX 78759

Dr. Holly Given
IGPP, A-025
Scripps Institute of Oceanography
University of California, San Diego
La Jolla, CA 92093

Dr. Jeffrey W. Given
SAIC
10260 Campus Point Drive
San Diego, CA 92121

Dr. Dale Glover
Defense Intelligence Agency
ATTN: ODT-1B
Washington, DC 20301

Dan N. Hagedon
Pacific Northwest Laboratories
Battelle Boulevard
Richland, WA 99352

Robert C. Kemerait
ENSCO, Inc.
445 Pineda Court
Melbourne, FL 32940

Dr. James Hannon
Lawrence Livermore National Laboratory
P.O. Box 808, L-205
Livermore, CA 94550

U.S. Dept of Energy
Max Koontz, NN-20, GA-033
Office of Research and Develop.
1000 Independence Avenue
Washington, DC 20585

Dr. Roger Hansen
University of Colorado, JSPC
Campus Box 583
Boulder, CO 80309

Dr. Richard LaCoss
MIT Lincoln Laboratory, M-200B
P.O. Box 73
Lexington, MA 02173-0073

Prof. David G. Harkrider
Division of Geological & Planetary Sciences
California Institute of Technology
Pasadena, CA 91125

Prof. Charles A. Langston
Geosciences Department
403 Deike Building
The Pennsylvania State University
University Park, PA 16802

Prof. Danny Harvey
University of Colorado, JSPC
Campus Box 583
Boulder, CO 80309

Jim Lawson, Chief Geophysicist
Oklahoma Geological Survey
Oklahoma Geophysical Observatory
P.O. Box 8
Leonard, OK 74043-0008

Prof. Donald V. Helmberger
Division of Geological & Planetary Sciences
California Institute of Technology
Pasadena, CA 91125

Prof. Thorne Lay
Institute of Tectonics
Earth Science Board
University of California, Santa Cruz
Santa Cruz, CA 95064

Prof. Eugene Herrin
Geophysical Laboratory
Southern Methodist University
Dallas, TX 75275

Dr. William Leith
U.S. Geological Survey
Mail Stop 928
Reston, VA 22092

Prof. Robert B. Herrmann
Department of Earth & Atmospheric Sciences
St. Louis University
St. Louis, MO 63156

Mr. James F. Lewkowicz
Phillips Laboratory/GPE
29 Randolph Road
Hanscom AFB, MA 01731-3010(2 copies)

Prof. Lane R. Johnson
Seismographic Station
University of California
Berkeley, CA 94720

Dr. Gary McCartor
Department of Physics
Southern Methodist University
Dallas, TX 75275

Prof. Thomas H. Jordan
Department of Earth, Atmospheric &
  Planetary Sciences
Massachusetts Institute of Technology
Cambridge, MA 02139

Prof. Thomas V. McEvilly
Seismographic Station
University of California
Berkeley, CA 94720

2

Dr. Keith L. McLaughlin
S-CUBED
A Division of Maxwell Laboratory
P.O. Box 1620
La Jolla, CA 92038-1620

Prof. Bernard Minster
IGPP, A-025
Scripps Institute of Oceanography
University of California, San Diego
La Jolla, CA 92093

Prof. Brian J. Mitchell
Department of Earth & Atmospheric Sciences
St. Louis University
St. Louis, MO 63156

Mr. Jack Murphy
S-CUBED
A Division of Maxwell Laboratory
11800 Sunrise Valley Drive, Suite 1212
Reston, VA 22091 (2 Copies)

Dr. Keith K. Nakanishi
Lawrence Livermore National Laboratory
L-025
P.O. Box 808
Livermore, CA 94550

Prof. John A. Orcutt
IGPP, A-025
Scripps Institute of Oceanography
University of California, San Diego
La Jolla, CA 92093

Dr. Howard Patton
Lawrence Livermore National Laboratory
L-025
P.O. Box 808
Livermore, CA 94550

Dr. Frank Pilotte
HQ AFTAC/TT
1030 South Highway A1A
Patrick AFB, FL 32925-3002

Dr. Jay J. Pulli
Radix Systems, Inc.
201 Perry Parkway
Gaithersburg, MD 20877

Prof. Paul G. Richards
Lamont-Doherty Earth Observatory
 of Columbia University
Palisades, NY 10964

Mr. Wilmer Rivers
Multimax Inc.
1441 McCormick Drive
Landover, MD 20785

Dr. Alan S. Ryall, Jr.
Lawrence Livermore National Laboratory
L-025
P.O. Box 808
Livermore, CA 94550

Dr.Chandan K. Saikia
Woodward Clyde- Consultants
566 El Dorado Street
Pasadena, CA 91101

Mr. Dogan Seber
Cornell University
Inst. for the Study of the Continent
3130 SNEE Hall
Ithaca, NY 14853-1504

Secretary of the Air Force
(SAFRD)
Washington, DC 20330

Office of the Secretary of Defense
DDR&E
Washington, DC 20330

Thomas J. Sereno, Jr.
Science Application Int'l Corp.
10260 Campus Point Drive
San Diego, CA 92121

Dr. Michael Shore
Defense Nuclear Agency/SPSS
6801 Telegraph Road
Alexandria, VA 22310

Prof. David G. Simpson
IRIS, Inc.
1616 North Fort Myer Drive
Suite 1050
Arlington, VA 22209

Dr. Jeffrey Stevens
S-CUBED
A Division of Maxwell Laboratory
P.O. Box 1620
La Jolla, CA 92038-1620

Prof. Brian Stump
Los Alamos National Laboratory
EES-3
 Mail Stop C-335
Los Alamos, NM 87545

Prof. Tuncay Taymaz
Istanbul Technical University
Dept. of Geophysical Engineering
Mining Faculty
Maslak-80626, Istanbul Turkey

Prof. M. Nafi Toksoz
Earth Resources Lab
Massachusetts Institute of Technology
42 Carleton Street
Cambridge, MA 02142

Dr. Larry Turnbull
CIA-OSWR/NED
Washington, DC 20505

Dr. Karl Veith
EG&G
5211 Auth Road
Suite 240
Suitland, MD 20746

Prof. Terry C. Wallace
Department of Geosciences
Building #77
University of Arizona
Tuscon, AZ 85721

Dr. William Wortman
Mission Research Corporation
8560 Cinderbed Road
Suite 700
Newington, VA 22122

ARPA, OASB/Library
3701 North Fairfax Drive
Arlington, VA 22203-1714

HQ DNA
ATTN: Technical Library
Washington, DC 20305

Defense Technical Information Center
Cameron Station
Alexandria, VA 22314 (2 Copies)

TACTEC
Battelle Memorial Institute
505 King Avenue
Columbus, OH 43201 (Final Report)

Phillips Laboratory
ATTN: GPE
29 Randolph Road
Hanscom AFB, MA 01731-3010

Phillips Laboratory
ATTN: TSML
5 Wright Street
Hanscom AFB, MA 01731-3004

Phillips Laboratory
ATTN: PL/SUL
3550 Aberdeen Ave SE
Kirtland, NM 87117-5776 (2 copies)

Dr. Michel Campillo
Observatoire de Grenoble
I.R.I.G.M.-B.P. 53
38041 Grenoble, FRANCE

Dr. Kin Yip Chun
Geophysics Division
Physics Department
University of Toronto
Ontario, CANADA

Prof. Hans-Peter Harjes
Institute for Geophysic
Ruhr University/Bochum
P.O. Box 102148
4630 Bochum 1, GERMANY

Prof. Eystein Husebye
NTNF/NORSAR
P.O. Box 51
N-2007 Kjeller, NORWAY

David Jepsen
Acting Head, Nuclear Monitoring Section
Bureau of Mineral Resources
Geology and Geophysics
G.P.O. Box 378, Canberra, AUSTRALIA

Ms. Eva Johannisson
Senior Research Officer
FOA
S-172 90 Sundbyberg, SWEDEN

Dr. Peter Marshall
Procurement Executive
Ministry of Defense
Blacknest, Brimpton
Reading FG7-FRS, UNITED KINGDOM

Dr. Bernard Massinon, Dr. Pierre Mechler
Societe Radiomana
27 rue Claude Bernard
75005 Paris, FRANCE (2 Copies)

Dr. Svein Mykkeltveit
NTNT/NORSAR
P.O. Box 51
N-2007 Kjeller, NORWAY (3 Copies)

Dr. Jorg Schlittenhardt
Federal Institute for Geosciences & Nat'l Res.
Postfach 510153
D-30631 Hannover , GERMANY

Dr. Johannes Schweitzer
Institute of Geophysics
Ruhr University/Bochum
P.O. Box 1102148
4360 Bochum 1, GERMANY

Trust & Verify
VERTIC
Carrara House
20 Embankment Place
London WC2N 6NN, ENGLAND